

Article

Synthetic and DFT Modeling Studies on Suzuki–Miyaura Reactions of 4,5-Dibromo-2-methylpyridazin-3(2*H*)-one with Ferrocene Boronates, Accompanied by Hydrodebromination and a Novel Bridge-Forming Annulation In Vitro Cytotoxic Activity of the Ferrocenyl–Pyridazinone Products

Nour-Eddine El Alaoui ¹, Mohammed Boulhaoua ¹, Dániel Hutai ¹, Rita Oláh-Szabó ², Szilvia Bősze ², Ferenc Hudecz ^{1,2} and Antal Csámpai ^{1,*}

¹ Department of Organic Chemistry, Institute of Chemistry, Eötvös Loránd University (ELTE), H-1117 Budapest, Hungary; nour-eddine1990@live.fr (N.-E.E.A.); mboulhaoua@student.elte.hu (M.B.); hutaidani@gmail.com (D.H.); ferenc.hudecz@ttk.elte.hu (F.H.)

² ELKH-ELTE Research Group of Peptide Chemistry, Eötvös Loránd Research Network (ELKH), Eötvös Loránd University (ELTE), Budapest Pázmány P. Sétány 1/A, H-1117 Budapest, Hungary; rita.szabo@ttk.elte.hu (R.O.-S.); szilvia.bosze@ttk.elte.hu (S.B.)

* Correspondence: csampai@caesar.elte.hu; Tel.: +36-1-372-2500-6591



Citation: Alaoui, N.-E.E.; Boulhaoua, M.; Hutai, D.; Oláh-Szabó, R.; Bősze, S.; Hudecz, F.; Csámpai, A. Synthetic and DFT Modeling Studies on Suzuki–Miyaura Reactions of 4,5-Dibromo-2-methylpyridazin-3(2*H*)-one with Ferrocene Boronates, Accompanied by Hydrodebromination and a Novel Bridge-Forming Annulation In Vitro Cytotoxic Activity of the Ferrocenyl–Pyridazinone Products. *Catalysts* **2022**, *12*, 578. <https://doi.org/10.3390/catal12060578>

Academic Editor: Werner Oberhauser

Received: 8 April 2022

Accepted: 20 May 2022

Published: 24 May 2022

Publisher's Note: MDPI stays neutral with regard to jurisdictional claims in published maps and institutional affiliations.



Copyright: © 2022 by the authors. Licensee MDPI, Basel, Switzerland. This article is an open access article distributed under the terms and conditions of the Creative Commons Attribution (CC BY) license (<https://creativecommons.org/licenses/by/4.0/>).

Abstract: This paper presented the efficiency of different Pd-based catalytic systems in a series of SM reactions of 4,5-dibromo-2-methylpyridazin-3(2*H*)-one with ferroceneboronic acid, ferrocene-1,1'-diboronoc acid, and its *bis*-pinacol ester. In addition to the disubstituted product, these transformations afford substantial amounts of isomeric 4- and 5-ferrocenyl-2-methylpyridazin-3(2*H*)-ones, and a unique asymmetric bi-pyridazinone-bridged ferrocenophane with a screwed molecular architecture. The reactions of phenylboronic acid, conducted under the conditions, are proven to be the most reductive in the conversions of ferroceneboronic acid, and produce 2-methyl-4,5-diphenylpyridazin-3(2*H*)-one as single product, supporting our view about solvent-mediated hydrodehalogenations that are supposed to proceed via the assistance of the ferrocenyl group present in the reaction mixture, or attached to the bromo-pyridazinone scaffold, which is constructed in the first SM coupling of the heterocyclic precursor. A comparative DFT modelling study on the structures and possible transformations of relevant bromo-, ferrocene- and phenyl-containing carbopalladated intermediate pairs was carried out, providing reasonable mechanisms suitable to account for the apparently surprising regioselectivity of the alternative hydrodebromination processes, and for the formation of the ferrocenophane product. Supporting the results of DFT modelling studies, the implication of DMF as a hydrogen transfer agent in the hydrodebromination reactions is evidenced by deuterium labelling experiments using the solvent mixtures DMF-*d*₇-H₂O (4:1) and DMF-D₂O (4:1). The organometallic products display antiproliferative effects on human malignant cell lines.

Keywords: Suzuki–Miyaura coupling; ferrocene; ferrocenophane; hydrodehalogenation; DFT-supported reaction mechanism; transmetalation; SET; Fe–Pd interaction; deuterium labeling experiments; NMR structural elucidation; antiproliferative activity

1. Introduction

During the last decades, the chemistry of ferrocenes attracted remarkable attention, due to their wide application in material sciences, catalysis, and the chemistry of bioactive compounds [1]. Focusing on the last characteristics, it was established that in certain bioactive compounds, the replacement of an aromatic/heteroaromatic ring for a ferrocene unit leads to organometallics possessing biological activity not manifested in, or superior to, those produced by the purely organic counterparts. This is most spectacularly

demonstrated by ferrocene-containing analogues of the non-steroidal selective estrogen receptor modulator hydroxytamoxifen, with strong cytotoxic and cytostatic effects on hormone-independent triple negative MDA-MB-231 breast tumour cells [2]. This tendency is further supported by a number of reviewed examples also presenting an array of organic ferrocene derivatives, with diverse scaffolds displaying pronounced antitumor activities [3,4]. The effect of ferrocene-based antiproliferative agents is mainly based on the generation of reactive oxygen species (ROS), such as nitric oxide, superoxide anion, and hydroxyl radical, which are involved in the Fenton pathway, causing DNA damage [5–7] and, eventually, leading to cell death. [8] Connecting to this emerging, but so far under-explored, research area, we also synthesized and evaluated a number of ferrocene-based hybrid compounds, comprised of building blocks with documented antiproliferative activity. Thus, cinchona-based diamides [9], triazolyl-calchones [10–12] imipridone hybrids [13], and polycondensed β -carboline [14] display substantial *in vitro* cytotoxicity against a variety of human malignant cell lines. On the other hand, structurally diverse pyridazine-containing heterocycles are privileged scaffolds in pharmaceutical chemistry. Although most of their well-documented bioactive representatives are found among anti-HIV [15], antiviral [16], antibacterial [17], antihypertensive [18], and anti-inflammatory [19] agents, certain pyridazine derivatives were also identified as anti-cancer drug candidates [20–24]. Since the chemistry and biological applications of ferrocene and pyridazine derivatives are the focus of our interest, we demonstrate that the chemical hybridization of ferrocene and pyridazinone moieties might result in highly promising complex organometallics, such as ferrocene-pyridazines comprising planar chiral scaffolds **I** [25], **II** [26], and isomeric diferrocenyl-substituted derivatives **III** and **IV** [27] that display significant antiproliferative effects on human malignant cell lines (Figure 1).

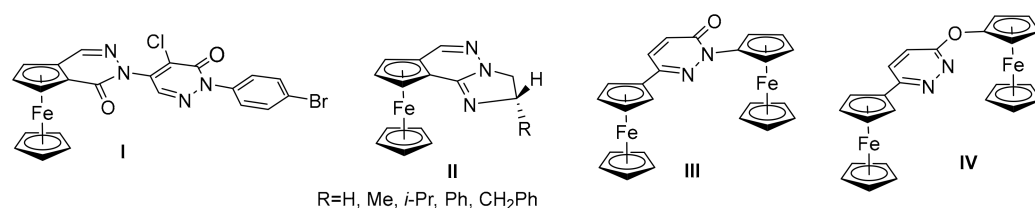


Figure 1. Ferrocene-containing pyridazine derivatives displaying antiproliferative effects on human malignant cell lines.

In the frame of our ongoing project of searching for more active compounds in this promising class of small molecules, we envisaged the synthesis, structural analysis, and *in vitro* anticancer evaluation of a series of further ferrocene-containing pyridazinone derivatives types **VI–VIII**, with structural characteristics complementary to those of **I–IV** (Figure 2).

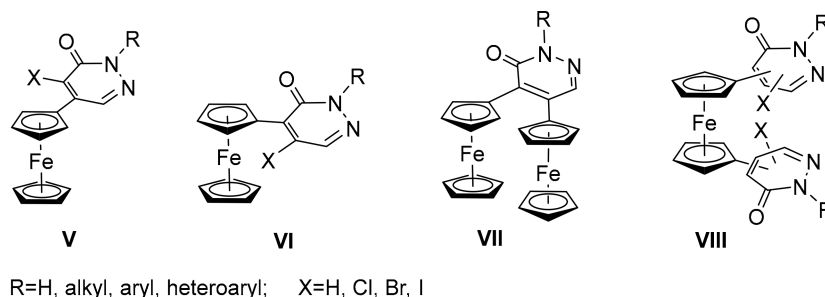


Figure 2. Types of the targeted ferrocene-containing pyridazinones structurally related to antiproliferative compounds **I–IV** (Figure 1).

A straightforward simple retrosynthetic analysis of the targeted structures suggests the utilisation of Suzuki–Miyaura (SM) reactions involving ferrocenyl–boron compounds and

4,5-dihalopyridazin-3(2*H*)-ones as coupling partners. Accordingly, in this contribution we present the first part of a systematic study on the aforementioned SM reactions, using different catalytic systems to promote the coupling of ferrocenylboronic acid (**1**), ferrocene-1,1'-diboronic acid (**2**), and ferrocene-1,1'-diboronic acid dipinacol ester (**3**) with 4,5-dibromo-2-methylpyridazin-3(2*H*)-one (**4**) (Figure 3). These mono- and bi-functionalized precursors are regarded as suitable models in a systematic series of experiments aimed at disclosing the structure–reactivity correlations related to the influence of the catalytic systems on the chemo- and regioselectivity in the reactions investigated.

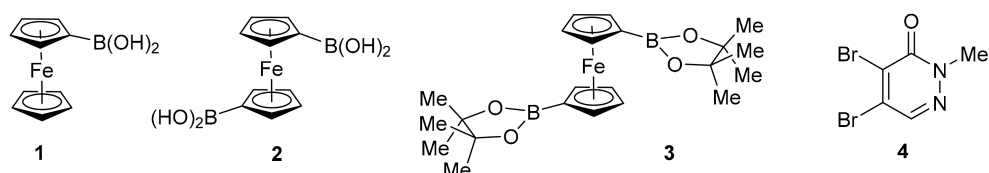
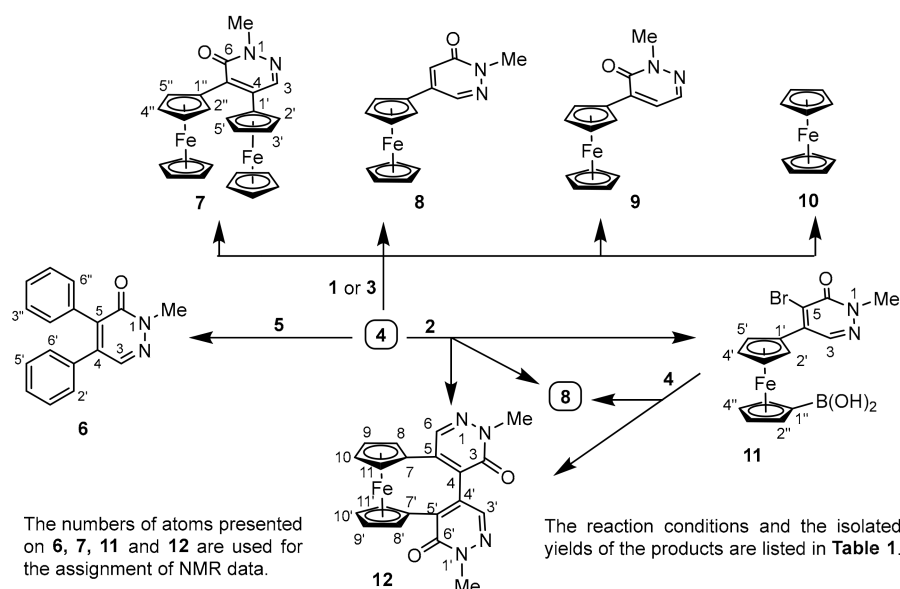


Figure 3. Precursors used in this work to construct the targeted types of ferrocene-containing pyridazinones **V–VIII** (Figure 2).

2. Results

Over the past decades, considerable research was devoted to an extremely wide array of catalytic systems and conditions evaluated in the SM reactions of organoboron compounds [28–44], including ferrocenyl–boronate components [32–38]. However, Stevenson et al. report on a closely related double SM coupling reaction of **4** with 3 equivalents of phenylboronic (**5**) acid, using $\text{PdCl}_2(\text{PPh}_3)_2$ as catalyst, Na_2CO_3 as a base, and $\text{DME–H}_2\text{O}$ as a solvent to afford the biarylated product **6** (Scheme 1) [28]. Since no detailed data on catalyst-loading, base amount, solvent mixture composition, reaction time, or temperature are provided, first, with the intention of coupling two phenyl groups to the pyridazinone core, we conducted this reference transformation at 100 °C for 10 h, employing a relatively high catalyst-loading (4%), 2.8 equivalents of the base, and a 4:1 mixture of the solvent components, and obtained **6** as exclusive product, isolated in 82% yield (Table 1, Method A).



Scheme 1. Suzuki–Miyaura coupling reactions of 4,5-dibromo-2-methylpyridazin-3(2*H*)-one (**4**) with phenyl- and ferrocene–boronates, conducted under the conditions listed in Table 1.

Table 1. Conditions and product distributions of the SM reactions of 4,5-dibromo-2-methylpyridazin-3(2H)-one **4** with phenylboronic acid **5**, and ferrocene-containing boronates **1–3**.

Entry	Reactants	Catalyst	Base	Solvent	Temp	Time	Method	Isolated Products [%]						
								6	7	8	9	10/X	11	12
1	4 + 5 ^a	PdCl ₂ (PPh ₃) ₂ (4 mol%)	Na ₂ CO ₃ (2.8 eq.)	DME–H ₂ O (4:1)	100 °C	10 h	A	82	-	-	-	-	-	-
2	4 + 1 ^a	PdCl ₂ (PPh ₃) ₂ (4 mol%)	Na ₂ CO ₃ (2.8 eq.)	DME–H ₂ O (4:1)	100 °C	10 h	A	-	26	6	18	7/15 ^c	-	-
3	4 + 1 ^a	Pd(PPh ₃) ₄ (4 mol%)	Na ₂ CO ₃ (3.0 eq.)	Toluene–H ₂ O (3:1)	100 °C	8 h	B	-	21	5	23s	5/20 ^c	-	-
4	4 + 1 ^a	Pd(PPh ₃) ₄ (4 mol%)	Na ₂ CO ₃ (3.0 eq.)	Toluene–H ₂ O (3:1)	100 °C	12 h	C	-	16	10	22	7/20 ^c	-	-
5	4 + 1 ^a	PdCl ₂ (PPh ₃) ₂ (4 mol%)	K ₂ CO ₃ (3.0 eq.)	DMF–H ₂ O (4:1)	80 °C	12 h	D	-	38	6	24	9/10 ^c	-	-
6	4 + 1 ^a	Pd–PEPPSI ^{iP} (4 mol%)	K ₂ CO ₃ (3.0 eq.)	DMF–H ₂ O (4:1)	80 °C	12 h	E	-	45	7	18	12/12 ^c	-	-
7	4 + 1 ^a	PdCl ₂ dppf (4 mol%)	K ₂ CO ₃ (3.0 eq.)	DMF–H ₂ O (4:1)	80 °C	12 h	F	-	5	18	50	7/-	-	-
8	4 + 5 ^a	PdCl ₂ dppf (4 mol%)	K ₂ CO ₃ (3.0 eq.)	DMF–H ₂ O (4:1)	80 °C	12 h	F	79	-	-	-	-/-	-	-
9	4 + 2 ^b	PdCl ₂ (PPh ₃) ₂ (4 mol%)	Na ₂ CO ₃ (2.8 eq.)	DME–H ₂ O (4:1)	100 °C	10 h	A	-	-	-	19	-/-	36	15
10	4 + 2 ^b	PdCl ₂ (PPh ₃) ₂ (4 mol%)	K ₂ CO ₃ (3.0 eq.)	DMF–H ₂ O (4:1)	80 °C	12 h	D	-	-	-	14	-/-	56	20
11	4 + 2 ^b	Pd–PEPPSI ^{iP} (4 mol%)	K ₂ CO ₃ (3.0 eq.)	DMF–H ₂ O (4:1)	80 °C	12 h	E	-	-	-	15	-/-	44	28
12	4 + 2 ^b	PdCl ₂ dppf (4 mol%)	K ₂ CO ₃ (3.0 eq.)	DMF–H ₂ O (4:1)	80 °C	12 h	F	-	-	-	47	-/-	7	9
13	4 + 11 ^a	PdCl ₂ (PPh ₃) ₂ (4 mol%)	K ₂ CO ₃ (3.0 eq.)	DMF–H ₂ O (4:1)	80 °C	12 h	D	-	-	34	-	-/-	27 ^d	24
14	4 + 11 ^a	Pd–PEPPSI ^{iP} (4 mol%)	K ₂ CO ₃ (3.0 eq.)	DMF–H ₂ O (4:1)	80 °C	12 h	E	-	-	14	-	-/-	10 ^d	21
15	4 + 11 ^a	PdCl ₂ dppf (4 mol%)	K ₂ CO ₃ (3.0 eq.)	DMF–H ₂ O (4:1)	80 °C	12 h	F	-	-	55	-	-/-	12 ^d	10
16	4 + 3 ^b	PdCl ₂ (PPh ₃) ₂ (4 mol%)	K ₂ CO ₃ (3.0 eq.)	DMF–H ₂ O (4:1)	80 °C	12 h	D	-	22	7	24	8/12 ^c	-	-
17	4 + 3 ^b	Pd–PEPPSI ^{iP} (4 mol%)	K ₂ CO ₃ (3.0 eq.)	DMF–H ₂ O (4:1)	80 °C	12 h	E	-	52	6	15	6/17 ^c	-	-
18	4 + 3 ^b	PdCl ₂ dppf (4 mol%)	K ₂ CO ₃ (3.0 eq.)	DMF–H ₂ O (4:1)	80 °C	12 h	F	-	5	9	42	14/8 ^c	-	-

^a 1/3. ^b 1/1.5. (molar ratios of the coupling components). ^c Yields of the recovered boronic acid/ester component [X = **1** (entries 2–7) or **11** (entries 13–15), or monopinacol ester derived from the partial hydrolysis of **3** (entries 16–18)] (calculated on the basis of the input amounts of the boronic component applied in excess). ^d Yield of the recovered precursor **11**.

Encouraged by the excellent performance of this methodology, we attempted to couple **4** with ferrocenylboronic acid **1** under the same conditions. To our surprise, besides the expected 4,5-diferroceno-2-methylpyridazin 3(2H)-one (**7**), the reaction leads to the isolation of the isomeric monoferrocenyl derivatives **8** and **9** in appreciable yields (with a marked dominance of **9**), along with a significant amount of ferrocene (**10**), which certainly originates from the undesired hydrolysis of **1** [36] (Table 1: entry 2, Method A). Following this unexpected outcome of our first experiment, we tested a variety of catalytic conditions to assess their efficiency and selectivity in the coupling of **4** and **1**. The reactions of these components were then run in the presence of Pd(PPh₃)₄ and Na₂CO₃ (3.0 equiv.), at 100 °C for 8–12 h in toluene–H₂O (3:1), the solvent mixture that facilitates aryl bromide activation [40]. Although these reactions are accompanied by the formation of tarry products, the use of

these conditions (Methods B and C) allows the isolation of the same products in yields and ratio comparable to those obtained using Method A (Table 1: entries 3 and 4). We attempted to increase the isolated yields of the targeted ferrocenylpyridazinones with the concomitant suppression of uncontrolled decompositions, by conducting the reactions at lowered temperature (80 °C) in the highly polar solvent mixture DMF–H₂O (4:1), which demonstrates robust character in related SM arylations [42,43]. In these experiments PdCl₂(PPh₃)₂, the emblematic air- and moisture-stable Pd–NHC, Pd–PEPPSI^{*i*-Pr} [44], and PdCl₂dppf were screened as catalysts in the presence of K₂CO₃ (3.0 equiv.) (entries 5–7, Methods D–F). Employing conditions in Methods D and E leads to the isolation of di-ferrocenylpyridazinone **7** as major product, along with the isomeric monoferrocenyl derivatives **8** and **9**, again with a marked preference of **9** (Entries 5 and 6), while PdCl₂dppf, featuring a chelate structure, almost entirely suppresses the formation of **7** and spectacularly promotes the formation of **8** and, in particular, **9**. These are accessed in markedly increased yields (Entry 7, Method F) compared to those achieved by Methods D and E. It must also be noted that under these conditions, independently of the structure of the catalyst used, hydrolytic deboration also takes place, to afford a significant amount of **10** (entries 5–7). In order to assess the influence of the structure of the boronate component on the outcome of the studied SM reactions, we also applied the conditions of Method F to couple **4** and phenylboronic acid **5**, and obtain di-phenylpyridazinone **6** as the single isolable product, in a 79% yield (entry 8), indirectly indicating the involvement of organometallic species in the observed dehydrobrominations, as discussed and reasoned in detail in the subsequent paragraph.

Aiming at the synthesis of target compounds with the general formula **VIII** (Figure 2) of potential antiproliferative activity, we attempted to couple **4** with ferrocene-1,1'-diboronic acid **2**, again using catalysts PdCl₂(PPh₃)₂, Pd–PEPPSI^{*i*-Pr}, and PdCl₂dppf, under the conditions of Methods A and D–F (Entries 9–12). To our surprise, besides **11**, one of the expected products, these reactions assemble a ferrocenophane-type product (**12**), featuring an asymmetrically connected bi-pyridazinone linker, in low-to-acceptable yields (9–28%), and **9** in characteristic catalyst-dependent yields (14–47%). On the other hand, the coupling reactions of **11** and **4**, run under the conditions of Methods D–F, again afford **12** and **8** in appreciable yields (entries 13–15), referring to a non-negligible propensity of the organometallic component to undergo hydrodebromination and hydrodeborylation.

Serving as control, the subsequent experiments were carried out under the conditions of Methods D–F, employing dipinacol ester **3** as the bifunctional boronate component, which demonstrates a reactivity profile surprisingly different from that of diboronic acid **2**, and similar to that of monoboronic acid **1**, as reflected in the catalyst-dependent product distributions (entries 16–18). The formation of **7**, **8**, **9**, and **10** points to an enhanced tendency of the boron–carbon bond to undergo hydrolytic cleavage in the primarily formed *mono*- and *bis*-ferrocenylpyridazinone intermediates, and even in **3** with bulky tetramethyl-1,3,2-dioxaborolene residues on the organometallic substituents, probably decreasing the steric congestion and, thus, increasing the rotational freedom of the cyclopentadienyl rings.

3. Discussion

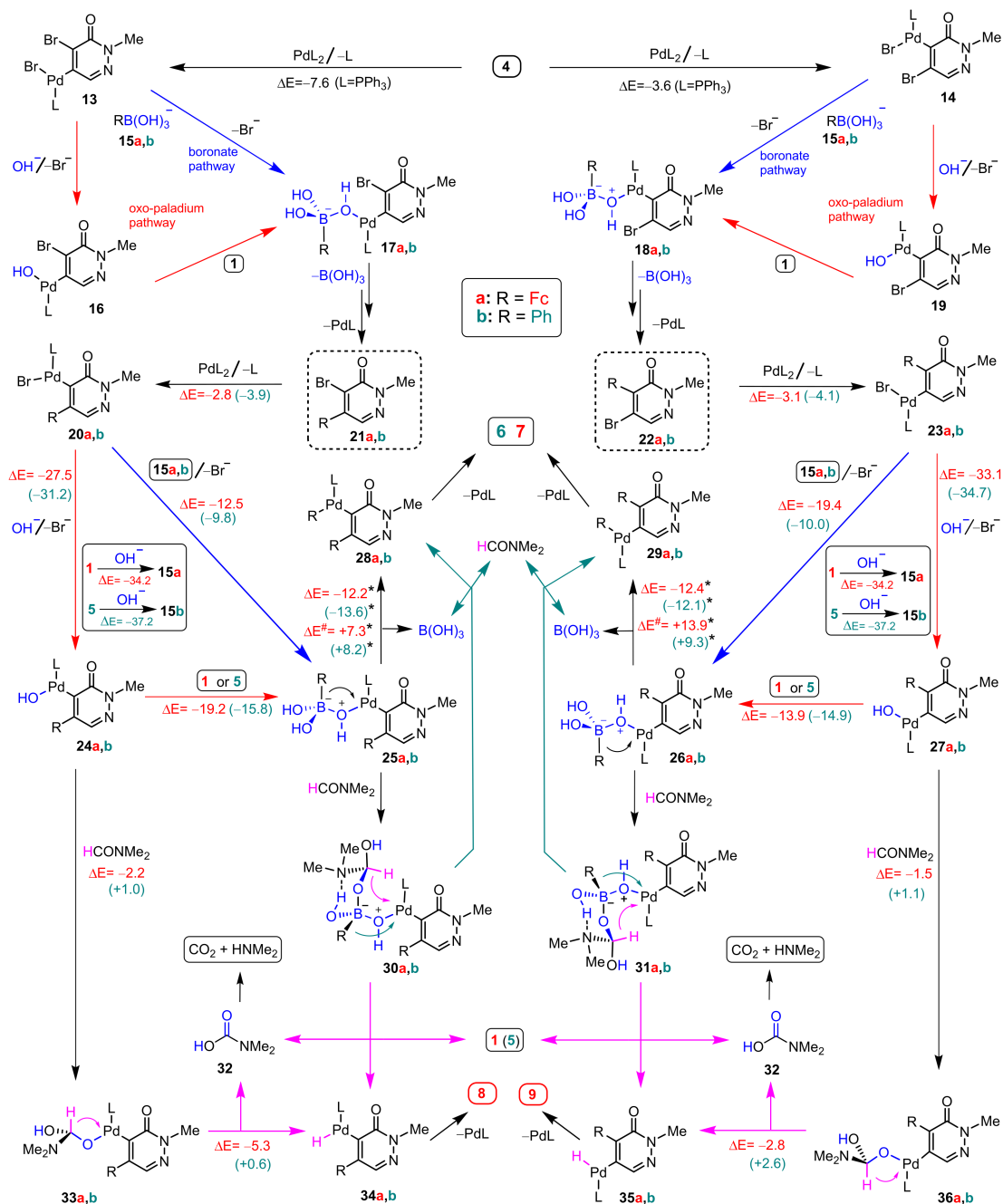
3.1. DFT-Modeled Possible Pathways of Sequential SM Coupling and Hydrodebromination Processes in the Reactions of **1** with Boronic Acids **2** and **5** Taking Place without Single Electron Transfer Steps

The straightforward, highly feasible, double coupling reactions **4** + **5** → **6**, along with the formation of unexpected dehydrobrominated products that accompany all the investigated SM reactions of **4** with ferrocene–boronates **1–3** and **11**, unambiguously imply the presence of the organometallic moiety in the reactants, and/or in the appropriate intermediates. First, in order to reveal the mode of a specific action of the primarily attached ferrocenyl group in the hydrodebromination processes, focusing on a possible competition between the second SM coupling and competitive hydrodebromination taking place under the conditions employing Pd-catalysts with PPh₃ ligand and DMF–H₂O (4:1) as solvent, we carried out a series of comparative DFT modeling studies on the most relevant elementary steps assumed to be involved in complex branched pathways (Scheme 2). All

calculations were performed using a B3PW91 functional [45] and DGTZVP basis set [46]. (Since the modeling studies were carried out also on organometallic species, we opted for B3PW91 as functional, as that is superior to B3LYP in providing a more reliable and realistic description of bonding parameters in metal-based fragments [47]. Providing further and, in terms of structural characteristics, more relevant justification for our choice of the DFT functional, it is also reported that the *N*-heterocyclic carbene complexes of Ni(II)-, Pd(II)-, and Pt(II), optimized by B3PW91, are closer to the experimental data relative to those found in the structures generated by B3LYP and M06 functionals [48].) First, the optimized structures were identified on the potential energy surface (PS) as local minima, or saddle points, for all the analyzed intermediates and transition states, respectively. The transition states of the investigated transmetalations were localized using the QST2 method [49]. The total energy values were then calculated from single point calculations performed on the structures, optimized in vacuo using the IEFPCM solvent model [50], and dielectric constant $\epsilon = 45.4$ estimated for DMF–H₂O (4:1), to represent the approximate polarity of the reaction mixture frequently applied in our experiments. The values referred to as relative energetics and presented in kcal/mol in the rest of discussion, and in Schemes 2–7, were obtained as the sum total energies of the precursor and product molecules involved in the particular reaction steps.

First, we calculated the energetic data of the alternative Pd(0)-mediated oxidative additions ($4 \rightarrow 13$ and $4 \rightarrow 14$: Scheme 2), which are correlated with the results of previous studies on nucleophilic functionalizations of 4,5-dibromopyridazinones, with preferred regioselectivity at position 5 [51–54]. The isomeric-carbopalladated intermediates **13** and **14** are supposed to convert into intermediates **17a,b** and **18a,b**, respectively, via two pathways first postulated for transmetalation by Suzuki and Miyaura [55]. Accordingly, the so-called “oxo-palladium pathway” is expected to involve Br \rightarrow OH exchange on the Pd-center, followed by the coordination of the boronic acid component (**1** or **5**) with the resulting hydroxy-palladium complexes **16** and **19**, while the alternative “oxoborate pathway” comprises the direct displacement of the bromide ligand in **13** and **14**, by the corresponding boronic, acid-derived, anionic hydroxyl adduct (**15a** or **15b**). This assumption is confirmed by the results of in-depth mechanistic studies [56–63], which establish that complexes featuring a palladium–oxygen–boron linkage are the species of outstanding propensity that undergo transmetalation proceeding through a four-membered transition state, as evidenced by DFT computations [61–63]. From this stage, focusing on the possible conversions of the isomeric monoaryl-substituted bromopyridazinones **21a,b** and **22a,b**, each elementary step was subjected to theoretical modeling to identify the critical elements that might be most significantly influenced by the structure of the primarily introduced aryl substituent (ferrocenyl or phenyl) in the selection between the second SM coupling and the appropriate hydrodebromination process. The energetic profiles of both oxo-palladium and boronate pathways refer to the highly favored formation of the pre-transmetalation intermediates **25a,b** and **26a,b**. In this context, it must also be pointed out that hydroxide-induced boronate generations $1 \rightarrow 15a$ and $5 \rightarrow 15b$ obviously connect the two pathways, as reflected in the thermochemical data calculated for these additions (Scheme 2). Modeling studies also demonstrate that **25a,b** and **26a,b** readily undergo energetically and kinetically feasible transmetalations with [1,3] aryl-migration ($25a,b \rightarrow 28a,b + H_3BO_3$ and $26a,b \rightarrow 29a,b + H_3BO_3$). The energetic profile, including activation barriers and the optimized structures involved in the transmetalation events (Scheme 3), share similar characteristics to those generated by Thomas et al. in the frame of an in-depth kinetic and computational study focusing on transmetalation in representative SM reactions [62]. Formally, **34a,b** and **35a,b** in principle, might also be constructed along pathways comprising the formation and subsequent boronate- and carbamate-generating fragmentation of highly complex, chelation-stabilized DMF-adducts, respectively, integrating an intramolecular [1,5]-hydride migration ($30a/31a \rightarrow 34a/35a + 1 + 32$ and $30b/31b \rightarrow 34b/35b + 5 + 32$). It is of note that [1,3] aryl-migrations in **30a,b** and **31a,b**, accompanied

by concomitant formation of boric acid and regeneration of DMF, also seem to be a feasible process to generate the aryl–palladium intermediates **28a,b** and **29a,b**, respectively.

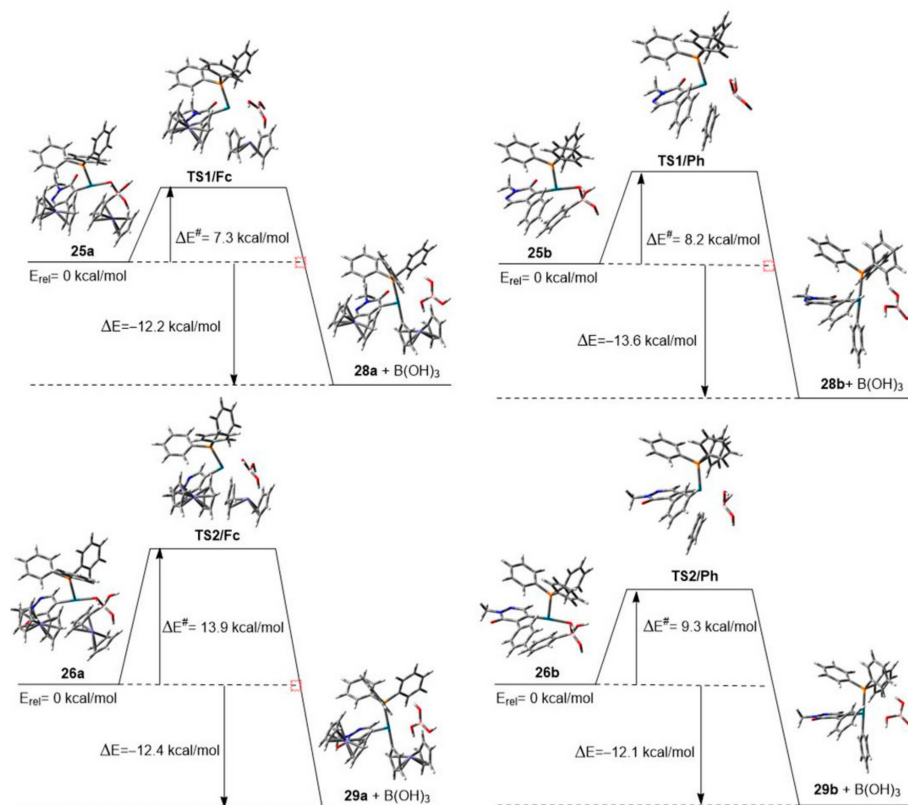


*Values referring to transmetalations taking place in **25a,b** and **26a,b** that directly construct molecular complexes **28a,b+B(OH)₃** and **29a,b+B(OH)₃**, respectively (optimized structures: cf. Scheme 3).

Scheme 2. The chart of DFT-modeled possible pathways without single electron transfer steps for sequential SM coupling reactions of **4** with **1** and **5**, respectively, aimed at disclosing the specific role of ferrocene moiety in the formation of **8** and **9**, under the conditions using Pd-catalysts with L = PPh₃ ligand and DMF–H₂O (4:1) as solvent. [The values of relative energetics (ΔE) and activation barriers (ΔE^\ddagger) (in kcal/mol) calculated for the analyzed elementary steps involving ferrocene- and phenyl-containing components are presented in red and (green), respectively].

Calculations disclose a favorable energetic profile for the two-step conversions of ferrocene-containing hydroxy–palladium intermediates **24a** and **27a**, assembling Pd-hydrides **34a** and **35a**, respectively. These transformations proceed via DMF addition, followed by

intramolecular carbon-to-palladium [1,3] hydride migration in adducts **33a** and **36a**, which take place simultaneously with fragmentation-generating carbamamic acid **32**, prone to undergo decomposition to Me_2NH and CO_2 . Terminating the hydrodebromination pathways, **34a** and **35a** are supposed to undergo reductive elimination to give **8** and **9**, respectively. Lending credence to the mechanism that involves DMF-adducts types **33** and **36**, there are examples in the literature reporting on transition-metal-catalyzed dehydrohalogenations proposed to proceed via intramolecular carbon-to-palladium [1,3] hydride migration in structurally related alkoxy-palladium intermediates, followed by sequence-terminating reductive elimination [64–70].



Scheme 3. Energetic profiles of transmetalation steps **25a,b** → **28a,b** and **26a,b** → **29a,b** proceeding via [1,3] carbon-to-palladium migration of ferrocenyl- and phenyl groups, as resulted from DFT modeling of the local minima and transition states.

The calculated energetic data suggest that the first two steps of the hydrodebromination pathway, starting from phenyl-substituted hydroxy-palladium intermediate **24b**, might also be regarded as operative, at least to a limited extent, while along the related pathway, the formation of Pd-hydride **35b** seems much less feasible. We assume that the energetically favored formation of **34a** and **35a** is assisted by the development of a stabilizing coordinative interaction between the donor ferrocene moiety and the adjacent Pd(II)-hydride fragment. Accordingly, MO analysis of their structures identified MOs showing significant electron delocalization over the proximal metal centers (with $\text{L} = \text{PPh}_3$; Figure 4). Donor-acceptor interactions with the coordinating phenyl group are also found in **34b** and **35b**, as visualized by the appropriate MOs (Figure 4), contributing to the stabilization of Pd-hydride structures, probably to a smaller extent compared to the interactions involving the ferrocenyl substituent in **34a** and **35a**. In line with our view about the development of the aforementioned intermetallic contact, ferrocene complexes featuring a $\text{Fe} \rightarrow \text{Pd}$ dative bond are well-documented in the literature [71–76]. On the other hand, MO analysis of complexes **13** and **14** ($\text{L} = \text{PPh}_3$) discloses definite Br-Pd interactions through a formal four-membered ring, as visualized by the MOs also presented in Figure 4. Thus, it

is postulated here that, in the modeled intermediates, either iron or bromine is regarded as the fourth ligand on the proximal Pd(II)-center, with an approximately square planar mode of coordination. It is also of note that definite interatomic contacts are also disclosed in intermediates **20a**, **23a**, **24a**, and **27a** between the ferrocenyl group and the proximal Pd–OH residue, as shown by the appropriate bonding MOs (collected in the Supplementary Material S3).

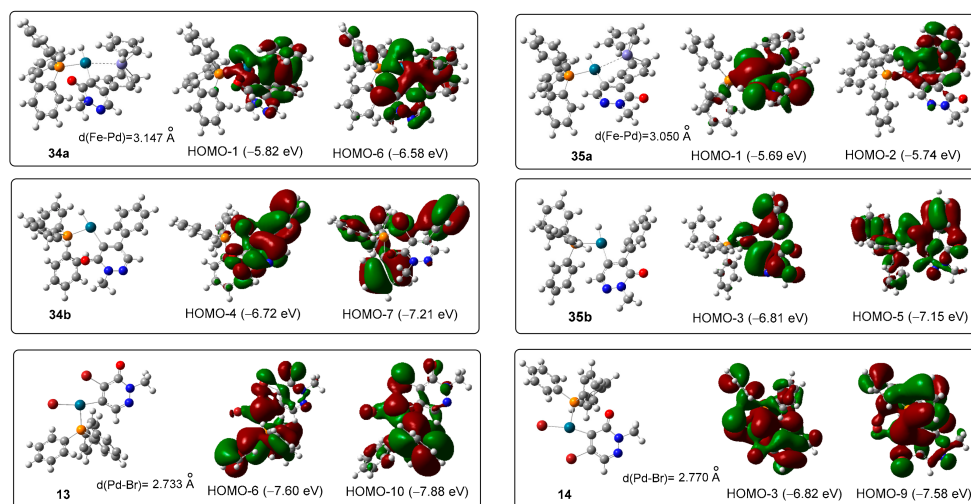
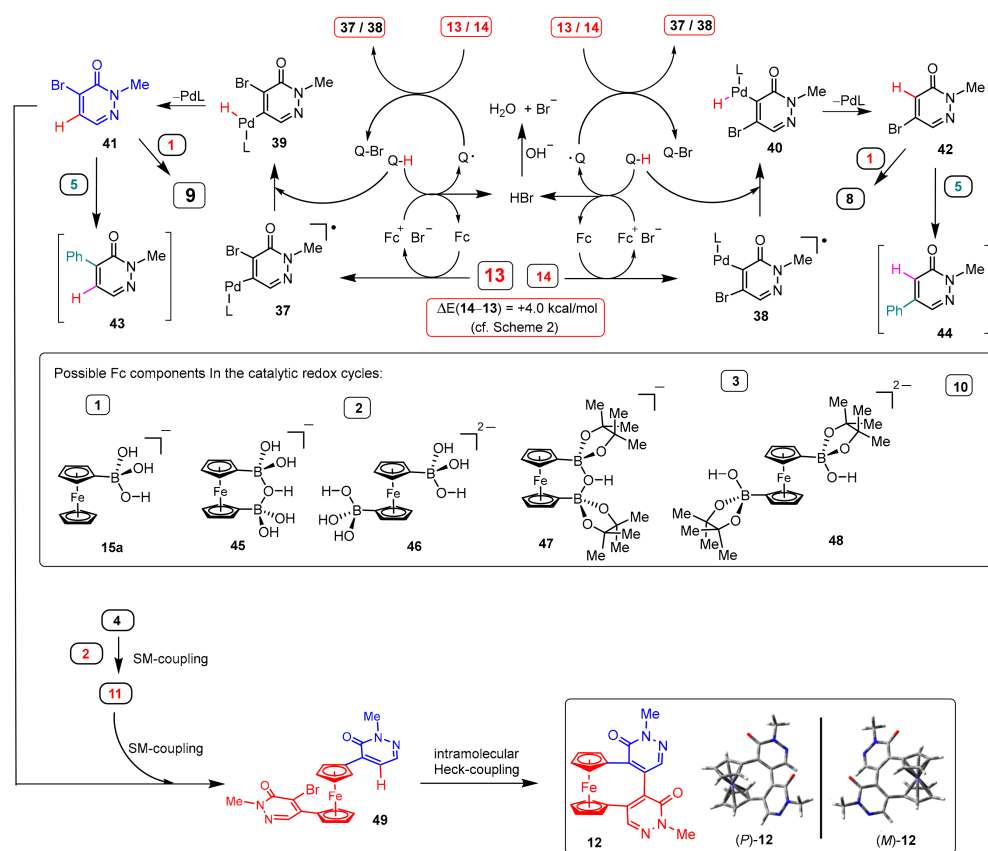


Figure 4. The identified sets of delocalized MOs indicating Fe–Pd interaction in ferrocene-containing complex isomer pair **34a** + **32**/**35a** + **32**, phenyl–Pd coordination interaction in phenyl-substituted complex isomer pair **34b** + **32**/**35b** + **32**, and Br–Pd interaction in bromo-substituted isomer pair **13**/**14**.

3.2. DFT-Modeled Possible Pathways of Hydrodebromination Processes Taking Place with Single Electron Transfer (SET) Steps Accompanying the Investigated SM Coupling Reactions

Up to this stage of modeling studies, in contrast to the experimental results, the energetic data and kinetic barriers calculated for the relevant conversions in the sequential transformations—with particular regard to the preference of oxidative addition **4** → **13** over the alternative elementary step **4** → **14** suggest the exclusive presence, or at least a marked dominance, of **8** over **9** in the isolated products of the reactions conducted under the conditions using DMF–H₂O (4:1) as solvent. Moreover, since the experimental product distribution is not significantly influenced by the solvent, it is reasonable to conclude that, besides the above-discussed pathways starting from the assumed 4/5-aryl-substituted 5/4-bromopyridazinones **21a,b** and **22a,b** (Scheme 2), further mechanisms must also be operative in hydrodebromination, which might correctly account for the preferred formation of **9** over that of **8**. Accordingly, we also propose competitive pathways (Scheme 4), which start with ferrocene-promoted bromine abstraction from **13** and **14**, resulting in the radical intermediates **37** and **38**, respectively. These events might involve any neutral ferrocene component (**1–3**, **10**) or boronate anions (**15a**, **45–48**) present in the reaction mixtures in different concentrations (Scheme 4), and are, in principle, capable of acting as a redox catalyst via single electron transfer (SET). In the subsequent step, from a suitable position of a solvent molecule (Q–H), a hydrogen atom is transferred to **37** and **38**, constructing the intermediates **39** and **40**, respectively, while simultaneously generating a carbon radical of solvent origin (Q). This carbon radical then effects bromine abstraction, either from the primary carbopalladated intermediate (**13** and **14**), or from the initially formed ferricenium bromide (Fc⁺Br[−]), to give a brominated solvent molecule (Q–Br), with simultaneous regeneration of the appropriate ferrocene-containing catalyst. It is assumed that the catalyst is also regenerated from the ferricenium bromide intermediate by a solvent molecule, again yielding the carbon radicals Q and HBr, which are then decomposed in the basic reaction mixture. When terminating the hydrodebromination pathways, Pd-hydrides **39** and **40**

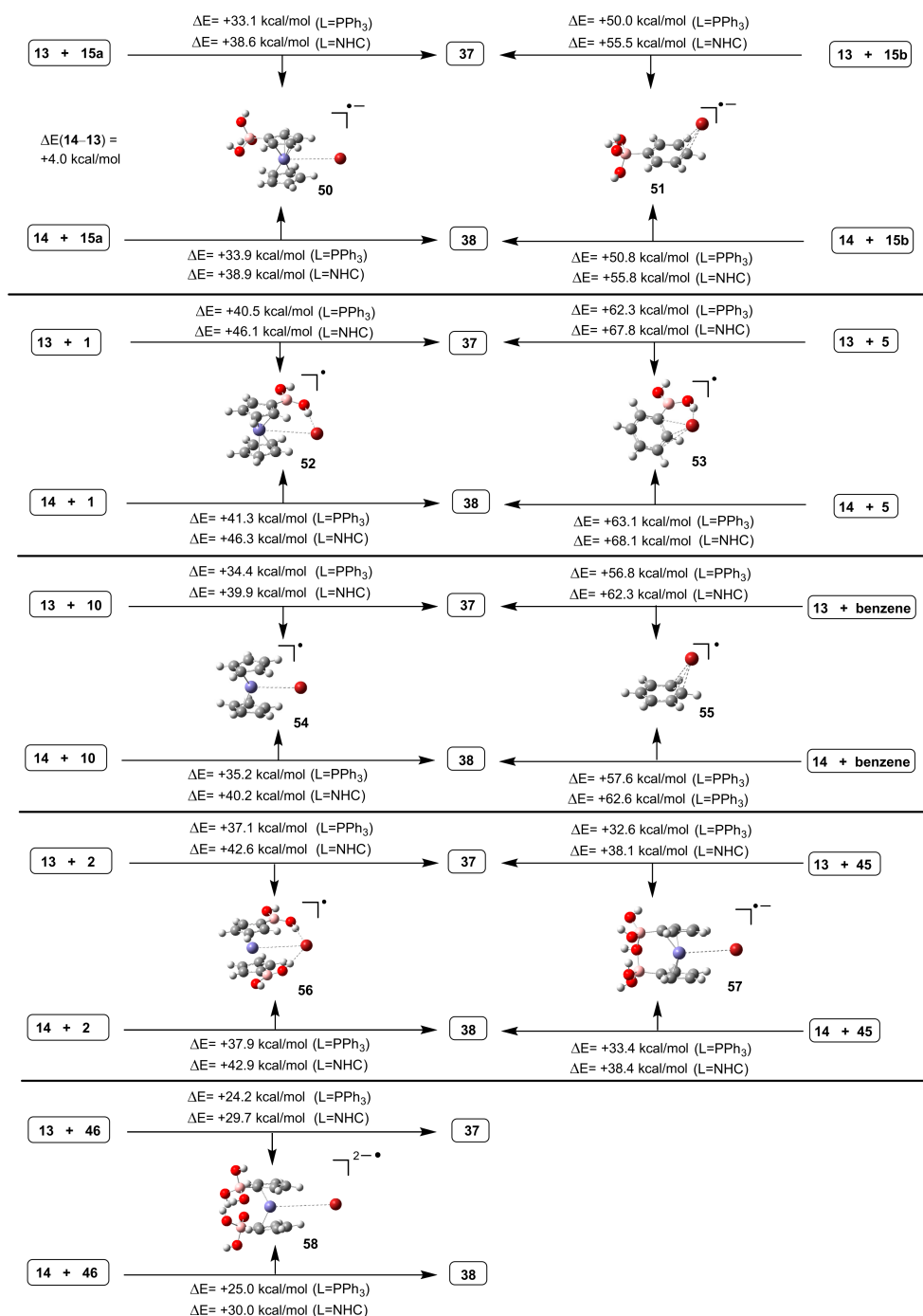
undergo reductive elimination to give the isomer bromopyridazinones **41** and **42**, certainly the actual organohalide coupling components that are involved in the SM reactions, finally leading to the formation of **9** and **8**, respectively. It is of pronounced importance that—due to the energetically controlled regioselectivity of the primary competitive oxidative additions $4 + \text{PdL}_2 \rightarrow 13 + \text{L}$, and $4 + \text{PdL}_2 \rightarrow 14 + \text{L}$ (cf. Scheme 2)—the previously discussed mechanism, with crucial SET events, is, at first sight, suitable to account for the preferred formation of **9** over **8**, the characteristic feature of the studied reactions practically invariant of the solvent used. Indirectly supporting our view about the mechanism discussed above, bromopyridazinones **41** and **42**, the simple coupling components, are not formed in the absence of ferrocene components. Accordingly, $^1\text{H-NMR}$ measurements detect neither of the isomer phenylpyridazinones **43** and **44**, even in traces, in the crude products of the reactions of **4** with phenylboronic acid **5**.



Scheme 4. The chart of possible solvent-invariant pathways to account for the formation of bridged ferrocenophane **12**, and for the experimentally observed chemo- and regioselectivity of hydrode-bromination, implicating radical bromine displacement associated with ferrocene-catalyzed single electron transfer (SET) steps. (The two conformationally rigid enantiomers of **12** with helical chirality, resulting from DFT-optimization, are also presented to emphasize that this product is formed as a racemic mixture).

The formation of ferrocenophane **12** can also be rationalized by the reaction sequence that involves SM reaction of **41** with **11**, followed by an intramolecular Heck-coupling taking place in the resulting *bis*-pyridazinone **49** (Scheme 4). The boronic component **11**, of the SM reaction, is formed in the SM-coupling of **4** and **2**, or used as reactant, while **41** is the practically exclusive, or at least the highly dominant, monohalide component in the reaction mixtures components, as a consequence of the substantially higher population of its radical precursor **13** relative to that of **4**, the radical precursor of the isomer monohalide **42**, as is concluded from the difference in their energy levels [$\Delta E(14 - 13) = +4.0 \text{ kcal/mol}$].

The influence of the structure of potential initiators on the relative feasibility of the initial radical transformations in the simple ferrocene–boronate-mediated reactions was estimated from the relative energetics, which were calculated for the series of bromine abstractions from **13** and **14** effected by representative ferrocene-containing components (**1**, **2**, **10**, **15a**, **45**, and **46**) of different electron donor strengths, along with **15b** and benzene as purely organic references (Scheme 5). In order to evaluate the effect of the ligand on the energetics, the bromine abstraction events were modeled using PPh_3 , 1,3-bis(2,6-diisopropylphenyl)imidazol-2-ylidene of Pd–PEPPSI^{*i*}-Pr-origin (NHC), and with dppf as ligand.

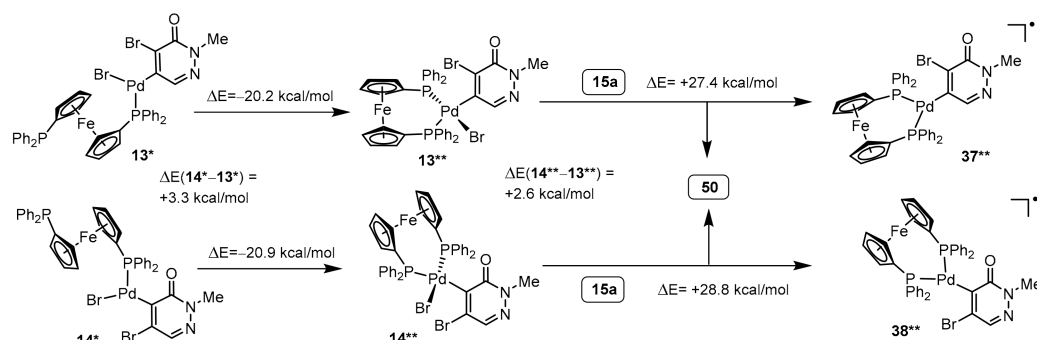


Scheme 5. Approximate assessment of the initiator and ligand dependence of the relative energetics of the crucial bromine radical transfers, as resulting from DFT calculations.

The calculated data indicate that anionic boronate **15a**, ferrocene (**10**) derived from hydrolytic deboronation, and the bridged monoboronate **45** have comparable efficiency in bromine abstraction taking place using the SET mechanism, and, in accord with the general expectations, diboronate **46** certainly presents in low concentrations in the reaction mixtures, and seems to be the most efficient reductant in the group of the modeled organometallics. On the other hand, **1** and **2**, with electron-deficient boron centers, are significantly less efficient reductants in the modeled elementary steps.

In this context, phenylboronate **15b** and benzene are identified as markedly weaker electron donors compared to their organometallic counterparts **15a** and **10**, respectively. All radical bromides are regarded as close ion pairs, whereas weak $\text{OH} \cdots \text{Br}$ interactions contribute to the stability of the boronate-derived neutral radicals **52**, **53**, and **56**, as reflected in their optimized structures.

The calculated energetic data also suggest that the coordinated PPh_3 is a slightly more efficient promoter of the critical bromine transfer than NHC, which facilitates SM reactions, rather than radical hydrodebromination, as reflected in the product distributions of the reactions catalyzed by $\text{Pd-PEPPSI}^{i\text{-Pr}}$ (Method E: Table 1). On the other hand, in accord with the high isolated yields of **9** achieved by the reactions catalyzed by PdCl_2dppf (Method F: Table 1), bromine transfer steps from the chelation-stabilized Pd-dppf complexes **13**** and **14**** become markedly more feasible compared to conversions **13** \rightarrow **17** and **14** \rightarrow **38**, as reflected in the relative energetics of boronate-mediated transformations **13**** \rightarrow **37**** and **14**** \rightarrow **38**** (Scheme 6). However, it is of pronounced importance that the energetic data determining the relative population of the isomer-carbopalladated complexes with dppf ligand [$\Delta E(\mathbf{14}^{**} - \mathbf{13}^{**}) = +2.6$ kcal/mol] refer again to the practically exclusive formation of **9**, via the SM coupling of 4-bromo-2-methylpyridazin-3(2*H*)-one **41** (Scheme 4), which is constructed by the sequential transformation of **13**** proceeding via radical intermediate **37****. At this stage of the discussion, it must be pointed out that, contrary to facile intramolecular chelation processes **13*** \rightarrow **13**** and **14*** \rightarrow **14**** (Scheme 6), the coordination of a second PPh_3 ligand to any of the carbopalladated complexes, with weakly interacting bromine or ferrocenyl groups as the fourth ligand in close proximity to the Pd(II) -center, is expected to be of highly limited probability, due to the low concentration of the species involved in this bimolecular event.

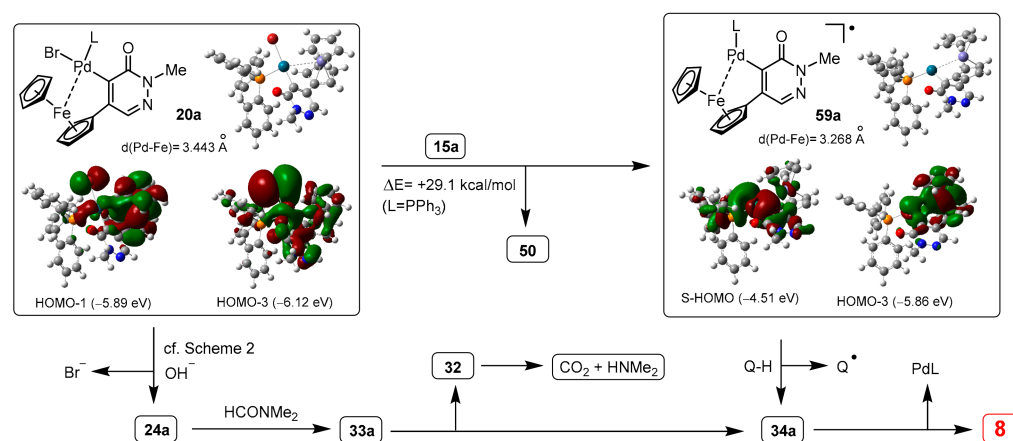


Scheme 6. Approximate assessment of the chelation-induced effect of the dppf ligand on energetics of the crucial bromine radical transfers, as resulting from DFT calculations.

On the basis of the previous discussions, it can be stated that, in all the investigated reactions, the fractions of **13** and **13**** escaping radical debromination enter boronate- or oxy-palladium pathways to assemble **21a**, the common precursor of the subsequent SM coupling and hydrodebromination, finally leading to **7** and **8**, respectively (Scheme 2). In this regard, it seems reasonable that **8** is formed along two competitive pathways branched from the Pd-Br complex **20a** (Scheme 6). Thus, besides the reaction sequence with intramolecular [1,3] hydride migration (**20a** \rightarrow **24a** \rightarrow **33** \rightarrow **34a**; Scheme 2), radical debromination (**20a** \rightarrow **55a**), followed by solvent-mediated hydrogen transfer, is also operative in the construction of palladium hydride **34a**, which decomposes by reductive elimination, affording

8 (Scheme 7). Accordingly, the change in energy calculated for the boronate-mediated radical debromination of **20a** indicates that the feasibility of this process is slightly increased, relative to that of the analogous conversion **13** + **15a** → **17** + **50** (Scheme 5), probably due to the strengthening of the Fe–Pd interaction upon the homolytic cleavage of the Pd–Br bond, as reflected in the intermetallic distances found in the optimized structures. This shortening might, at least partly, be ascribed to the significant spin-density delocalized between the adjacent metal centers shown by S-HOMO in **59a**. Delocalization of HOMO-3 also contributes to the Fe–Pd bonding order in this radical, while in **20a**, this interatomic contact is mainly the consequence of the HOMO-3 delocalization, with a lower energy level.

In the light of the experimental results supported by modeling-based theoretical considerations, it is reasonable to assume that, under the conditions using DMF–H₂O (4:1) as solvent, both pathways lead to the formation of **8** in a competitive manner, while the radical mechanism might only be considered as operative in the other solvents used in our synthetic procedures.



Scheme 7. The two pathways leading to the formation 5-ferrocenylpyridazin-3(2H)-one **8**, presented with the changes in energy and in Fe–Pd distance accompanying the radical bromine transfer step. The visualized MO's are involved in the intermetallic contact in the bromo–palladium and radical complexes.

Finally, it must be pointed out that the energetic data calculated for the endoergic radical bromine transfer processes suggest that these transformations are not feasible at all. However, on the one hand, the reagent- and ligand-dependent relative feasibility of these processes is clearly reflected in the results, which are roughly compatible with the experimental product distributions. On the other hand, under real experimental conditions, in the presence of a large number of solvent molecules with significant coordination and solvation ability, the relative energetics might significantly differ from the calculated values, allowing the development of an equilibrium system containing the highly reactive radical carbopalladated intermediates, in concentrations sufficient to advance the sequential transformations towards the formation of monoferrocenyl pyridazinone products **8** and **9**.

3.3. Deuterium Labelling Experiments Disclosing the Implication of DMF as Hydrogen Source in the Hydrodebromination Processes

Attempting to obtain conclusive experimental evidence for the theoretically established mechanisms of DMF-mediated hydrodebromination processes, we performed deuterium labelling experiments, by coupling **4** with **1** under the conditions of Method F (proven to be the most efficient method among the tested conditions in terms of hydrodebromination) in solvent mixtures DMF-*d*₇-H₂O (4:1) and DMF-D₂O (4:1), to check the implication of DMF as the source of hydride anion or atomic hydrogen in the ionic and radical pathways, respectively. Supporting the theoretically proposed mechanisms, the reaction conducted in the first solvent mixture **8** (yield: 15%) and **9** (yield: 46%) are isolated

in isotopically labelled forms, deuterated at positions 5 and 4, respectively, as identified by ^1H - and ^{13}C -NMR (cf. Section 3.4). On the other hand, indirectly referring to the practically exclusive implication of DMF as hydrogen transfer agent, when DMF– D_2O (4:1) is used as solvent, **8** (yield: 20%) and **9** (yield: 53%) are isolated in deuterium-free forms, as also detected by NMR methods. In both experiments, **7** is isolated in low yields (5–8%) in deuterium-free form.

3.4. Structural Elucidation of Ferrocenylpyridazinones 7–9, 11, and Ferrocenophane 12

The ^1H - and ^{13}C -NMR data of the novel ferrocene-substituted pyridazinone products are consistent with their structures, but the following remarks are necessary to make. The unambiguous assignments of the ^1H - and ^{13}C -NMR signals are confirmed by 2D-HSQC-, HMBC-, and NOESY measurements. In the ^1H -NMR spectrum of **8**, the split of 1.5 Hz of the H-3 and H-5 signals indicates the separated 1,3-skeletal position of the involved protons on the pyridazinone ring, whereas in the ^1H -NMR spectrum of **9**, the split of 4.3 Hz measured for the doublets originates from H-3 and H-4, and indicates their adjacent position. Providing further support for the substituent pattern in **8**, NOE interactions are detected for both the following signal pairs: H-3/H-2',5' and H-5/H-2',5'. The arrangement of the substituents on the pyridazinone ring in boronic acid **11** is evidenced by the NOE interaction detected between signal pairs H-3/H-2',5' and $\text{B}(\text{OH})_2/\text{H-2',5'}$. The assignment of H-5 signal in **8** is confirmed by its characteristic HMBC cross-peak correlation with the C-6 signal, mediated by two bonds, whereas no similar correlation is discernible between H-3 and C-6, separated by four bonds on pyridazinone ring. On the other hand, in the ^1H - ^{13}C -HMBC spectrum of **9**, a three-bond-mediated intense cross-peak correlation is detected between the signals of H-4 and C-6. The rigid bridged constitution of **12** is reflected in the six separated signals in the ^1H -NMR spectrum (with intensity distribution of 1H, 2H, 1H, 1H, 2H, and 1H), and ten separated signals in the ^{13}C -NMR spectrum, originating from the non-inverting ferrocene moiety in the chiral molecular architecture. The asymmetric constitution and the screwed conformation are confirmed by the NOEs detected between signal pairs H-6/H-8 and H-3'/ CH_3 on N-2.

Due to the lack of $^4J(\text{H-D})$ coupling, and to the negligible $^3J(\text{H-D})$ coupling, the H-3 signal is discernible as a singlet at 7.86 ppm and 7.65 ppm in the ^1H -NMR spectra of **8**(D-5) and **9**(D-4), respectively; these products formed in the experiment carried out by Method E in DMF- d_7 - H_2O (4:1). Accordingly, the signals of the deuterated carbons in the ^{13}C -NMR spectra [discernible at 120.8 ppm for **8**(D-5) and 123.8 ppm for **9**(D-4)] split into a 1:1:1 triplet, of which peaks are separated by 22.4–22.6 Hz corresponding to $^1J(^{13}\text{C-D})$ coupling (see in Supplementary Materials S2). The further ^1H - and ^{13}C -NMR data of **8**(D-5) and **9**(D-4) are practically identical to those measured for their deuterium-free counterparts.

4. In Vitro Evaluation of the Ferrocene-Containing Pyridazinones for Their Antiproliferative Activity

By means of MTT assay, the cytostatic effect of the novel organometallic heterocycles was studied in vitro on A2058 human melanoma [77], A431 human epidermoid carcinoma [78], U87 human glioma [79], and HepG2 human hepatocellular carcinoma [80] cell lines. In order to estimate the contribution of the ferrocenyl-substituent(s) to the bioactivity, 4,5-diphenylpyridazin-3(2H)-one **6** was used as purely organic reference. The data listed in Table 2 indicate that the investigated organometallic models display marked cell-line-dependent cytotoxicity; however, **6** exhibits no detectable effect in the assays, even at 50 μM concentration, underlying the essential role of the ferrocenyl substituent(s) in triggering antiproliferative activity at cellular level. Contrary to human melanoma A2058 cells, which are susceptible only to di-ferrocenyl-pyridazinone **7**, all the ferrocene-derivatives are active against human epidermoid carcinoma A431 cells at a low micromolar range, as shown by the IC_{50} values. Further demonstrating the cell line dependence of the antiproliferative activity of these members of ferrocenylpyridazinones, U87 human glioma cells display insensitivity to the investigated compounds, whereas the HepG2 cell line is susceptible to

compounds **7**, **9**, and **12**. In our experiments, compound **7** is identified as the most active model, referring again to the critical role of the organometallic moiety in triggering the antiproliferative effect. It is worth pointing out that the bridged ferrocenophane **12** also seems a highly promising lead, as this chiral compound with helical conformation displays significant antiproliferative effects, even in racemic form. Thus, with the intention to study the control of absolute configuration on bioactivity, we initiated attempts to separate the enantiomers of **12**. These experiments are currently in progress.

Table 2. Cytostatic activity of ferrocene-containing pyridazinones **7**, **8**, **9**, **11**, and **12**, and the reference 4,5-diphenylpyridazin-3(2H)-one **6**, expressed in IC₅₀ values on four human tumor cell lines.

Compounds	IC ₅₀ [μM] ± SD			
	A2058	A431	U87	HepG2
7	12.20 ± 0.28	1.82 ± 0.01	>50	2.57 ± 0.33
8	>50	45.68 ± 4.84	>50	>50
9	>50	5.16 ± 0.34	>50	3.61 ± 0.62
11	>50	10.38 ± 0.52	>50	>50
12	>50	2.93 ± 0.11	>50	2.49 ± 0.19
6 (reference)	>50	>50	>50	>50

5. Materials and Methods

All fine chemicals were obtained from commercially available sources (Merck, Budapest, Hungary; Molar Chemicals, Budapest, Hungary; VWR, Budapest, Hungary) and were used without further purification. Dichloromethane (DCM) was distilled and then stored on CaH₂. Merck Kieselgel (230–400 mesh, 60 Å) was used for flash column chromatography. Melting points (uncorrected) were determined with a M-560 instrument (Büchi, Essen, Germany). The ¹H- and ¹³C-NMR spectra were recorded in CDCl₃ or DMSO-*d*₆ solution in 5 mm tubes, at room temperature, on a Bruker DRX-500 spectrometer (Bruker Biospin, Karlsruhe, Germany) at 500 (¹H) and 125 (¹³C) MHz, with the deuterium signal of the solvent as the lock and TMS as internal standard (¹H, ¹³C). The 2D-NOESY, HSQC, and HMBC spectra were obtained by using the standard Bruker pulse programs. Since the performance of 2D-NOESY was poor in case of **12**, the stereostructure of this compound was investigated by 1D-NOEDIFF spectroscopy, using the standard Bruker pulse program. All calculations were carried out using the Gaussian 09 software (Gaussian Incorporation, Pittsburgh, PA, USA) package [81]. The optimized structures are available from the authors.

5.1. General Procedure for the Suzuki–Miyaura Reaction of 4,5-Dibromo-2-methylpyridazin-3(2H)-one **4** with Boronic Components **1**, **2**, **3**, **5**, and **11**

Under a flow of argon 4,5-dibromo-2-methylpyridazin-3(2H)-one **4** (536 mg, 2 mmol), boronic component (1.380 g, 6 mmol of **1**; 1.644 g, 6 mmol of **2**; 2.628 g, 6 mmol of **3**; 732 mg, 3 mmol of **5**; 1.251 g, 3 mmol of **11**), base (594 mg, 5.6 mmol of Na₂CO₃ by Method A; 830 mg, 6.0 mmol of K₂CO₃ by Methods B–F), and 4 mol% of the catalyst (56 mg, of PdCl₂(PPh₃)₂ by Methods A and D; 93 mg of Pd(PPh₃)₄ by Methods B and C; 55 mg of Pd-PEPPSI^{IP} by Method E; 59 mg of PdCl₂dppf by Method F) were suspended in the solvent [30 mL of DME–H₂O (4:1) by Method A; 32 mL of toluene–H₂O (3:1) by Methods B and C; 30 mL of DMF–H₂O (4:1) by Methods D–F], placed in a round-bottomed 100 mL two-necked vessel equipped with a reflux condenser and a gas inlet tube. The mixture was saturated with argon for 10 min, then stirred at elevated temperature for a prolonged time (data are given in Table 1). The reaction mixture was concentrated in vacuo, triturated with water, and carefully neutralized by 10% aqueous HCl. The precipitated solid was filtered off, dried under vacuo, and subjected to column chromatography on silica using solvent mixtures CH₂Cl₂–MeOH (50:1–80:1) as eluent, to obtain the corresponding product. The isolated yields are listed in Table 1. (To achieve sufficient separation of the organometallic components in the visible yellow-to-red colored bands, the ratio of the separable mixture to silica was set at least to 1 g:70 g). The crude solid resulting from the reactions of **1** and

phenylboronic acid **5** was purified by crystallization with MeOH–H₂O (1:10) to obtain 2-methyl-4,5-diphenylpyridazin-3(2H)-one **6** as a single product.

5.1.1. 2-Methyl-4,5-diphenylpyridazin-3(2H)-one (**6**)

White powder. M.p. 178–180 °C. ¹H-NMR (CDCl₃): 7.84 (s, 1H, H-3); 7.10–7.06 (m, 2H, H-2',6'); 7.26–7.16 (m, 8H, H-3'-5',2'-6'); 3.85 (s, 3H, CH₃ on N-1). ¹³C-NMR (CDCl₃): 160.6 (C-6); 140.9 (C-4); 138.1 (C-3); 137.0 (C-5); 135.2 (C-1'); 132.6 (C-1'); 130.5 (C-2',6'); 129.1 (C-2',6'); 128.6 (C-4'); 128.5 (C-3',5'); 128.3 (C-4'); 127.9 (C-3',5'); 40.7 (CH₃ on N-1). Anal. calcd. for C₁₇H₁₄N₂O: C, 77.84%; H, 5.38%; N, 10.68%. Found: C, 77.53%; H, 5.60%; N, 10.81%.

5.1.2. 4,5-Diferrocenyl-2-methylpyridazin-3(2H)-one (**7**)

Orange–red powder. M.p. 155–157 °C. ¹H-NMR (CDCl₃): 7.96 (s, 1H, H-3); 4.45 (t, *J* = 1.8 Hz, 2H, H-2',5'); 4.27 (t, *J* = 1.8 Hz, 2H, H-2',5'); 4.24 (t, *J* = 1.8 Hz, 2H, H-3',4'); 4.21 (t, *J* = 1.8 Hz, 2H, H-3',4'); 4.05 and 4.01 (2xs, 2x5H; 2xη⁵-C₅H₅); 3.80 (s, 3H, CH₃ on N-1). ¹³C-NMR (CDCl₃): 159.2 (C-6); 139.2 (C-3); 137.8 (C-4); 134.8 (C-5); 81.6 (C-1'); 78.0 (C-1'); 72.0 (C-3',4'); 70.05 (C-3',4'); 69.94 and 69.84 (2xη⁵-C₅H₅); 69.1 (C-2',5'); 68.7 (C-2',5'); 40.3 (CH₃ on N-1). (Anal. calcd. for C₂₅H₂₂Fe₂N₂O: C, 62.80%; H, 4.64%; N, 5.86%. Found: C, 62.50%; H, 4.72%; N, 6.01%.

5.1.3. 4-Ferrocenyl-2-methylpyridazin-3(2H)-one (**8**)

Orange–red powder. M.p. 188–190 °C. ¹H-NMR (CDCl₃): 7.80 (d, *J* = 1.5 Hz; 1H, H-3); 6.81 (d, *J* = 1.5 Hz; 1H, H-5); 4.61 (t, *J* = 1.8 Hz, 2H, H-2',5'); 4.46 (t, *J* = 1.8 Hz, 2H, H-3',4'); 4.09 (s, 5H; η⁵-C₅H₅); 3.73 (s, 3H, CH₃ on N-1). ¹³C-NMR (CDCl₃): 160.8 (C-6); 145.3 (C-4); 135.6 (C-3); 120.6 (C-5); 77.0 (C-1'); 71.2 (C-3',4'); 70.1 (η⁵-C₅H₅); 67.2 (C-2',5'); 40.0 (CH₃ on N-1). Anal. calcd. for C₁₅H₁₄FeN₂O: C, 61.25%; H, 4.80%; N, 9.52%. Found: C, 60.92%; H, 4.92%; N, 9.33%.

5.1.4. 5-Ferrocenyl-2-methylpyridazin-3(2H)-one (**9**)

Orange powder. M.p. 134–137 °C. ¹H-NMR (CDCl₃): 7.61 (d, *J* = 4.3 Hz; 1H, H-3); 7.22 (d, *J* = 4.3 Hz; 1H, H-4); 5.08 (t, *J* = 1.8 Hz, 2H, H-2',5'); 4.45 (t, *J* = 1.8 Hz, 2H, H-3',4'); 4.09 (s, 5H; η⁵-C₅H₅); 3.82 (s, 3H, CH₃ on N-1). ¹³C-NMR (CDCl₃): 159.9 (C-6); 140.7 (C-5); 136.0 (C-3); 123.6 (C-4); 77.2 (C-1'); 71.0 (C-3',4'); 70.0 (η⁵-C₅H₅); 69.2 (C-2',5'); 40.8 (CH₃ on N-1). Anal. calcd. for C₁₅H₁₄FeN₂O: C, 61.25%; H, 4.80%; N, 9.52%. Found: C, 61.11%; H, 4.95%; N, 9.65%.

5.1.5. [1'-(5-Bromo-1-methyl-6-oxo-1,6-dihydropyridazin-4-yl)ferrocenyl]boronic Acid (**11**)

Deep red powder. M.p. 211–215 °C. ¹H-NMR (DMSO-*d*₆): 8.04 (s, 1H, H-3); 7.53 [s, 2H, B(OH)₂]; 4.89 (br s, 2H, H-2',5'); 4.45 (br s, 2H, H-3',4'); 4.38 (br s, 2H, H-2',5'); 4.32 (br s, 2H, H-3',4'); 3.64 (s, 3H, CH₃ on N-1). ¹³C-NMR (DMSO-*d*₆): 157.2 (C-6); 144.0 (C-4); 137.5 (C-3); 121.2 (C-5); 78.0 (C-1'); 76.1 (C-2',5'); 73.9 (C-3',4'); 71.6 (C-3',4'); 71.0 (C-2',5'); 67.3 (C-1'); 41.0 (CH₃ on N-1). Anal. calcd. for C₁₅H₁₄BBrFeN₂O₃: C, 43.22%; H, 3.39%; N, 6.72%; Br 19.17%. Found: C, 43.75%; H, 3.48%; N, 6.44; Br 19.04%.

5.1.6. 1',2-Dimethyl-5,5'-(ferrocene-1,1'-diyl)-(4,4'-bipyridazine)-3,6'-(1'H,2H)-dione (**12**)

Brownish red powder. M.p. 237–240 °C. ¹H-NMR (CDCl₃): 7.73 (s, 1H, H-6); 7.57 (s, 1H, H-3'); 4.99 (br s, 1H, H-8'); 4.93 (narrow overlapping m's, 2H, H-10, and H-10'); 4.42 (dd, *J* = 1.6 Hz and 1.1 Hz, 1H, H-11'); 4.30 (dd, *J* = 1.6 Hz and 1.1 Hz, 1H, H-8); 4.23 (dd, *J* = 1.6 Hz and 1.1 Hz, 1H, H-11); 4.08 (narrow overlapping m's, 2H, H-9, and H-9'); 3.81 (s, 3H, CH₃ on N-1'); 3.85 (s, 3H, CH₃ on N-2). ¹³C-NMR (CDCl₃): 159.8 (C-6'); 159.2.9 (C-3); 143.5 (C-5); 139.0 (C-3'); 137.9 (C-5'); 136.8 (C-6); 132.8 (C-4'); 128.9 (C-4); 80.8 (C-11); 79.2 (C-11'); 77.2 (C-8'); 75.6 (C-10); 73.3 (C-7); 71.9 (C-7'); 71.0 (C-9'); 70.7 (C-9); 69.7 (C-10'); 66.0 (C-8); 41.3 (CH₃ on N-2); 41.1 (CH₃ on N-1'). Anal. calcd. for C₂₀H₁₆FeN₄O₂: C, 60.02%; H, 4.03%; N, 14.00%. Found: C, 59.89%; H, 4.09%; N, 14.41%.

5.2. Description of In Vitro Cytostasis Experiments

A2058 and HepG2 cells were cultured in RPMI-1640 medium, supplemented with 10% FCS (fetal calf serum, Sigma-Aldrich Ltd., Budapest, Hungary), 2 mM L-glutamine, penicillin–streptomycin antibiotics mixture (50 IU/mL and 50 µg/mL, respectively). A431 and U87 cells were cultured in DMEM medium, supplemented with 10% FBS, 2 mM L-glutamine, penicillin–streptomycin antibiotics mixture (50 IU/mL and 50 µg/mL, respectively), 1 mM sodium pyruvate, and 1% non-essential amino acid mixture. The cultures were maintained at 37 °C in a humidified atmosphere with 5% CO₂. The cells were grown to confluency, and then they were divided into 96-well tissue culture plates, with the initial cell number of 5.0×10^3 cells/well. After 24 h incubation at 37 °C, the cells were treated with the compounds in 200 µL final volume, containing 1.0 v/v% DMSO, at 0.4–50 µM concentration range overnight, whereas control cells were treated with serum-free medium only, or with DMSO (c = 1.0 v/v%) under the same conditions. After incubation, cells were washed twice with serum-free medium. Following that, cells were cultured for further 72 h in 10% serum containing medium at 37 °C, then MTT-solution (at c = 0.37 mg/mL final concentration) was added to each well. The respiratory chain [81], and other electron transport systems [82], reduce MTT and form non-water-soluble violet formazan crystals within the cell [83]. The amount of these crystals was determined by spectrophotometry, and served as an estimate for the number of mitochondria and, hence, the number of living cells in the well [84,85]. After 3 h of incubation with MTT, the cells were centrifuged for 5 min at $900 \times g$, and then the supernatant was removed. The obtained formazan crystals were dissolved in DMSO (100 µL), and optical density (OD) of the samples was measured at $\lambda = 540$ nm and 620 nm, using ELISA Reader (iEMS Reader, Labsystems Diagnostics Oy, Vantaa, Finland). OD₆₂₀ values were subtracted from OD₅₄₀ values. The percent of cytostasis was calculated with the following equation:

$$\text{Cytostatic effect (\%)} = [1 - (\text{OD}_{\text{treated}}/\text{OD}_{\text{control}})] \times 100$$

where values OD_{treated} and OD_{control} correspond to the optical densities of the treated and the control wells, respectively. In each case, two independent experiments were carried out with 4 parallel measurements. Cytostasis was plotted as a function of concentration, and the half maximal inhibitory concentration was calculated based on a sigmoid curve fitted on the data points using Microcal™ Origin2018 software. IC₅₀ represents the concentration of a compound that is required for 50% inhibition, expressed in micromolar units.

6. Conclusions

This contribution presents a detailed synthetic and mechanistic study on the complex transformations of 4,5-dibromo-pyridazin-3(2H)-one, an apparently simple heterocyclic bifunctional building block, with ferrocene-containing boronate components. It was established that the expected double Suzuki–Miyaura reactions run in water-containing solvent mixtures are accompanied by hydrodebromination processes, specifically promoted by the primarily introduced ferrocenyl group in the appropriate bromo–pyridazinone intermediate, or by a ferrocene-containing species present in the reaction mixture. The catalyst-dependent experimental product distributions are correlated with the relative energetics of the critical elementary steps and regioisomer key intermediates of the competitive polar and radical multistep reaction pathways. We also recognized and rationalized a bridge-forming annulation that assembled the first representative of a novel class of heterocyclic ferrocenophanes featuring asymmetric constitution, with rigid chiral conformation. Even in racemic form, this compound demonstrates antiproliferative activity in low micromolar concentration against two human malignant cell lines (A431 and HepG2). Pointing to the essential role of the organometallic moiety in triggering cytotoxicity, 2-methyl-4,5-diphenylpyridazin-3(2H)-one (6) is identified as an inactive organic reference, whereas its differrocenyl counterpart (7) displays substantial cell-line selective effect under in vitro conditions. The family of the ferrocene-containing anticancer pyridazinones presented in

this contribution can be extended by the replacement of the *N*-methyl group for an array of substituents, including privileged building blocks found in documented therapeutic agents. The experimentally and theoretically disclosed effects of the reaction conditions and catalysts on product distribution can be utilized in the design of synthetic protocols.

Supplementary Materials: The following supporting information can be downloaded at: <https://www.mdpi.com/article/10.3390/catal12060578/s1>, S1: Copies of the 1D- and 2D-NMR spectra. S2: Copies of the ¹H-, ¹³C NMR spectra of the deuterated products. S3: Bonding orbitals contributing to Fe–Pd interaction in compounds **20a**, **23a**, **24a**, and **27a**. S4: XYZ coordinates of the structures optimized by B3PW91/DGTZVP method.

Author Contributions: Conceptualization, A.C. and F.H.; methodology, N.-E.E.A., M.B., D.H., A.C., R.O.-S. and S.B.; software, A.C. and S.B.; validation, S.B. and R.O.-S.; formal analysis, S.B. and R.O.-S.; investigation, N.-E.E.A., M.B., D.H., R.O.-S. and A.C.; resources, A.C.; data curation, N.-E.E.A., M.B., D.H., S.B. and A.C. writing—original draft preparation, N.-E.E.A. and A.C.; writing—review and editing, F.H. and A.C.; visualization, A.C.; supervision, F.H.; project administration, D.H.; funding acquisition, A.C. All authors have read and agreed to the published version of the manuscript.

Funding: This research was financially supported by the Hungarian Scientific Research Fund [OTKA K_129037], Hungary, and by the ELTE Thematic Excellence Program, supported by the Hungarian Ministry for Innovation and Technology [SzintPlusz_1117].

Institutional Review Board Statement: Not applicable.

Informed Consent Statement: Not applicable.

Data Availability Statement: The data generated and analyzed during our research are not available in any public database or repository, but will be shared by the corresponding author upon reasonable request.

Acknowledgments: We thank Cintia Jernei-Duró and Lucia Kotasková for the technical assistance in the synthetic work.

Conflicts of Interest: The authors declare no conflict of interest.

References

1. Togni, A.; Hayashi, T. *Ferrocenes: Homogeneous Catalysis, Organic Synthesis, Materials Science*; VCH Publishers: New York, NY, USA, 1995; ISBN 9783527290482. [[CrossRef](#)]
2. Jaouen, G.; Top, S.; Vessières, A.; Alberto, R. New paradigms for synthetic pathways inspired by bioorganometallic chemistry. *J. Organomet. Chem.* **2000**, *600*, 23–36. [[CrossRef](#)]
3. Ornelas, C. Application of ferrocene and its derivatives in cancer research. *New J. Chem.* **2011**, *35*, 1973–1985. [[CrossRef](#)]
4. Braga, S.S.; Silva, A.M.S. A New Age for Iron: Antitumoral Ferrocenes. *Organometallics* **2013**, *32*, 5626–5639. [[CrossRef](#)]
5. Tamura, H.; Miwa, M. DNA Cleaving Activity and Cytotoxic Activity of Ferricenium Cations. *Chem. Lett.* **1997**, *26*, 1177–1178. [[CrossRef](#)]
6. Houlton, A.; Roberts, R.; Silver, J. Studies on the anti-tumour activity of some iron sandwich compounds. *J. Organomet. Chem.* **1991**, *418*, 107–112. [[CrossRef](#)]
7. Osella, D.; Ferrali, M.; Zanello, P.; Laschi, F.; Fontani, M.; Nervi, C.; Cavgiolio, G. On the mechanism of the antitumor activity of ferrocenium derivatives. *Inorganica Chim. Acta* **2000**, *306*, 42–48. [[CrossRef](#)]
8. Simon, H.-U.; Haj-Yehia, A.; Levi-Schaffer, F. Role of reactive oxygen species (ROS) in apoptosis induction. *Apoptosis* **2000**, *5*, 415–418. [[CrossRef](#)]
9. Károlyi, B.I.; Bősze, S.; Orbán, E.; Sohár, P.; Drahos, L.; Gál, E.; Csámpai, A. Acylated mono-, bis- and tris- Cinchona-Based Amines Containing Ferrocene or Organic Residues: Synthesis, Structure and in Vitro Antitumor Activity on Selected Human Cancer Cell Lines. *Molecules* **2012**, *17*, 2316–2329. [[CrossRef](#)]
10. Kocsis, L.L.; Szabó, I.; Bosze, S.; Jernei, T.; Hudecz, F.; Csámpai, A. Synthesis, structure and in vitro cytostatic activity of ferrocene–Cinchona hybrids. *Bioorg. Med. Chem. Lett.* **2016**, *26*, 946–949. [[CrossRef](#)]
11. Podolski-Renić, A.; Bősze, S.; Dinić, J.; Kocsis, L.; Hudecz, F.; Csámpai, A.; Pešić, M. Ferrocene–cinchona hybrids with triazolyl-chalcone linkers act as pro-oxidants and sensitize human cancer cell lines to paclitaxel. *Metallomics* **2017**, *9*, 1132–1141. [[CrossRef](#)]
12. Latif, A.D.; Jernei, T.; Podolski-Renić, A.; Kuo, C.-Y.; Vágvölgyi, M.; Girst, G.; Zupkó, I.; Develi, S.; Ulukaya, E.; Wang, H.-C.; et al. Protoflavone-Chalcone Hybrids Exhibit Enhanced Antitumor Action through Modulating Redox Balance, Depolarizing the Mitochondrial Membrane, and Inhibiting ATR-Dependent Signaling. *Antioxidants* **2020**, *9*, 519. [[CrossRef](#)]

13. Bárány, P.; Oláh, R.S.; Kovács, I.; Czuczi, T.; Szabó, C.L.; Takács, A.; Lajkó, E.; Láng, O.; Kóhidai, L.; Schlosser, G.; et al. Ferrocene-Containing Impiridone (ONC201) Hybrids: Synthesis, DFT Modelling, In Vitro Evaluation, and Structure–Activity Relationships. *Molecules* **2018**, *23*, 2248. [[CrossRef](#)]
14. Fodor, K.J.; Hutai, D.; Jernei, T.; Takács, A.; Szász, Z.; Sulyok-Eiler, M.; Harmat, V.; Szabó, R.O.; Schlosser, G.; Hudecz, F.; et al. Novel Polycondensed Partly Saturated β -Carbolines Including Ferrocene Derivatives: Synthesis, DFT-Supported Structural Analysis, Mechanism of Some Diastereoselective Transformations and a Preliminary Study of their In Vitro Antiproliferative Effects. *Molecules* **2020**, *25*, 1599. [[CrossRef](#)]
15. Akahane, A.; Katayama, H.; Mitsunaga, T.; Kato, T.; Kinoshita, T.; Kita, Y.; Kusunoki, T.; Terai, T.; Yoshida, K.; Shiokawa, Y. Discovery of 6-Oxo-3-(2-phenylpyrazolo[1,5-a]pyridin-3-yl)-1(6H)-pyridazinebutanoic Acid (FK 838): A Novel Non-Xanthine Adenosine A1 Receptor Antagonist with Potent Diuretic Activity. *J. Med. Chem.* **1999**, *42*, 779–783. [[CrossRef](#)]
16. Meade, E.A.; Wotring, L.L.; Drach, J.C.; Townsend, L.B. Synthesis and Antiproliferative and Antiviral Activity of Carbohydrate-Modified Pyrrolo[2,3-d]pyridazin-7-one Nucleosides. *J. Med. Chem.* **1997**, *40*, 794–801. [[CrossRef](#)]
17. Kimura, T.; Fujihara, Y.; Shibakawa, N.; Fujiwara, H.; Itoh, E.; Matsunobu, K.; Tabata, K.; Yasuda, H. Pyrrolopyridazine Derivatives. U.S. Patent 6063782 A, 17 July 1996.
18. Siddiqui, A.A.; Mishra, R.; Shaharyar, M. Synthesis, characterization and antihypertensive activity of pyridazinone derivatives. *Eur. J. Med. Chem.* **2010**, *45*, 2283–2290. [[CrossRef](#)]
19. Refaat, H.M.; Khalil, O.M.; Kadry, H.H. Synthesis and anti-inflammatory activity of certain piperazinythienylpyridazine derivatives. *Arch. Pharm. Res.* **2007**, *30*, 803–811. [[CrossRef](#)]
20. Malinka, W.; Redzicka, A.; Lozach, O. New derivatives of pyrrolo [3,4-d]pyridazinone and their anticancer effects. *Farmaco* **2004**, *59*, 457–462. [[CrossRef](#)]
21. Jiang, J.; Boxer, M.B.; van der Heiden, M.G.; Shen, M.; Skoumbourdis, A.P.; Southall, N.; Veith, H.; Leister, W.; Austin, C.P.; Park, H.W.; et al. Evaluation of thieno [3,2-b]pyrrole [3,2-d]pyridazinones as activators of the tumor cell specific M2 isoform of pyruvate kinase. *Bioorg. Med. Chem. Lett.* **2010**, *20*, 3387–3393. [[CrossRef](#)]
22. Abd El-Ghaffar, N.F.; Mohamed, M.K.; Kadah, M.S.; Radwan, A.M.; Said, G.H.; Abd Al, S.N. Synthesis and antitumor activities of some new pyridazinones containing the 2-phenyl-1H-indolyl moiety. *J. Chem. Pharm. Res.* **2011**, *3*, 248–259.
23. Rathish, I.; Javed, K.; Ahmad, S.; Bano, S.; Alam, M.; Akhter, M.; Pillai, K.; Ovais, S.; Samim, M. Synthesis and evaluation of anticancer activity of some novel 6-aryl-2-(p-sulfamylphenyl)-pyridazin-3(2H)-ones. *Eur. J. Med. Chem.* **2012**, *49*, 304–309. [[CrossRef](#)]
24. Gutierrez, D.A.; DeJesus, R.E.; Contreras, L.; Rodriguez-Palomares, I.A.; Villanueva, P.J.; Balderrama, K.S.; Monterroza, L.; Larragoity, M.; Varela-Ramirez, A.; Aguilera, R.J. A new pyridazinone exhibits potent cytotoxicity on human cancer cells via apoptosis and poly-ubiquitinated protein accumulation. *Cell Biol. Toxicol.* **2019**, *35*, 503–519. [[CrossRef](#)]
25. Csókás, D.; Zupkó, I.; Károlyi, B.I.; Drahos, L.; Holczbauer, T.; Palló, A.; Czugler, M.; Csámpai, A. Synthesis, spectroscopy, X-ray analysis and in vitro antiproliferative effect of ferrocenylmethylene-hydrazinylpyridazin-3(2H)-ones and related ferroceno[d]pyridazin-1(2H)-ones. *J. Organomet. Chem.* **2013**, *743*, 130–138. [[CrossRef](#)]
26. Csókás, D.; Károlyi, B.I.; Bősze, S.; Szabó, I.; Báti, G.; Drahos, L.; Csámpai, A. 2,3-Dihydroimidazo[1,2-b]ferroceno[d]pyridazines and a 3,4-dihydro-2H-pyrimido[1,2-b]ferroceno[d]pyridazine: Synthesis, structure and in vitro antiproliferation activity on selected human cancer cell lines. *J. Organomet. Chem.* **2014**, *750*, 41–48. [[CrossRef](#)]
27. Jernei, T.; Bősze, S.; Szabó, R.; Hudecz, F.; Majrik, K.; Csámpai, A. N-ferrocenylpyridazinones and new organic analogues: Synthesis, cyclic voltammetry, DFT analysis and in vitro antiproliferative activity associated with ROS-generation. *Tetrahedron* **2017**, *73*, 6181–6192. [[CrossRef](#)]
28. Stevenson, T.M.; Crouse, B.A.; Thieu, T.V.; Gebreysus, C.; Finkelstein, B.L.; Sethuraman, M.R.; Dubas-Cordery, C.M.; Piotrowski, D.L. Application of cross-coupling and metalation chemistry of 3(2H)-pyridazinones to fungicide and herbicide discovery. *J. Heterocycl. Chem.* **2005**, *42*, 427–435. [[CrossRef](#)]
29. Kadu, B.S. Suzuki–Miyaura cross coupling reaction: Recent advancements in catalysis and organic synthesis. *Catal. Sci. Technol.* **2021**, *11*, 1186–1221. [[CrossRef](#)]
30. Shaaban, M.R.; Farghaly, T.A.; Khormi, A.Y.; Farag, A.M. Recent Advances in Synthesis and Uses of Heterocycles-based Palladium(II) Complexes as Robust, Stable, and Low-cost Catalysts for Suzuki–Miyaura Crosscouplings. *Curr. Org. Chem.* **2019**, *23*, 1601–1662. [[CrossRef](#)]
31. Pagett, A.B.; Lloyd-Jones, G.C. Suzuki–Miyaura Cross-Coupling. *Org. React.* **2019**, *100*, 547–620. [[CrossRef](#)]
32. Knapp, R.; Rehahn, M. Palladium-catalyzed arylation of ferrocene derivatives: A convenient high yield route to 1,1'-bis(halophenyl)ferrocenes. *J. Organomet. Chem.* **1993**, *452*, 235–240. [[CrossRef](#)]
33. Imrie, C.; Loubser, C.; Engelbrecht, P.; McClelland, C.W. The use of a modified Suzuki reaction for the synthesis of monoarylferrocenes. *J. Chem. Soc. Perkin Trans.* **1999**, *1*, 2513–2523. [[CrossRef](#)]
34. Hua, D.H.; McGill, J.W.; Lou, K.; Ueki, A.; Helfrich, B.; Desper, J.; Zanello, P.; Cinquantini, A.; Corsini, M.; Fontani, M. Parallel and perpendicular stacking of ferrocene rings.: Syntheses, X-ray structures, and electrochemistry of 1,8-bis-[1-(1'-phenylthio)ferrocenyl]naphthalene and 8,8'-bis-[1-(1'-phenylthio)ferrocenyl]-1,1'-binaphthyl. *Inorganica Chim. Acta* **2003**, *350*, 259–265. [[CrossRef](#)]
35. Köcher, S.; Lutz, M.; Spek, A.L.; Prasad, R.; van Klink, G.P.; van Koten, G.; Lang, H. Heterobimetallic Fe–Pd and Fe–Pt NCN pincer complexes (NCN=[C₆H₂(CH₂NMe₂)₂-2,6][−]). *Inorganica Chim. Acta* **2006**, *359*, 4454–4462. [[CrossRef](#)]

36. Cammidge, A.N.; Scaife, P.J.; Berber, G.; Hughes, D.L. Cofacial Porphyrin–Ferrocene Dyads and a New Class of Conjugated Porphyrin. *Org. Lett.* **2005**, *7*, 3413–3416. [[CrossRef](#)] [[PubMed](#)]
37. Braga, D.; Polito, M.; Braccacini, M.; D’Addario, D.; Tagliavini, E.; Sturba, L.; Grepioni, F. Novel Organometallic Building Blocks for Molecular Crystal Engineering. 2. Synthesis and Characterization of Pyridyl and Pyrimidyl Derivatives of Diboronic Acid, $[\text{Fe}(\eta^5\text{-C}_5\text{H}_4\text{-B}(\text{OH})_2)_2]$, and of Pyridyl Boronic Acid, $[\text{Fe}(\eta^5\text{-C}_5\text{H}_4\text{-4-C}_5\text{H}_4\text{N})(\eta^5\text{-C}_5\text{H}_4\text{-B}(\text{OH})_2)]$. *Organometallics* **2003**, *22*, 2142–2150. [[CrossRef](#)]
38. Braga, D.; D’Addario, D.; Polito, M.; Grepioni, F. Mechanically Induced Expedient and Selective Preparation of Disubstituted Pyridine/Pyrimidine Ferrocenyl Complexes. *Organometallics* **2004**, *23*, 2810–2812. [[CrossRef](#)]
39. Peña-Cabrera, E.; Aguilar-Aguilar, A.; González-Domínguez, M.; Lager, E.; Zamudio-Vázquez, R.; Godoy-Vargas, J.; Villanueva-García, F. Simple, General, and Efficient Synthesis of Meso-Substituted Borondipyromethenes from a Single Platform. *Org. Lett.* **2007**, *9*, 3985–3988. [[CrossRef](#)]
40. Wern, C.; Ehrenreich, C.; Joosten, D.; Stein, T.V.; Buchholz, H.; König, B. Rapid Access to Bi- and Tri-Functionalized Dibenzofurans and their Application in Selective Suzuki–Miyaura Cross Coupling Reactions. *Eur. J. Org. Chem.* **2018**, *2018*, 5644–5656. [[CrossRef](#)]
41. Schulz, J.; Horký, F.; Čisáňová, I.; Štěpnička, P. Synthesis, Structural Characterization and Catalytic Evaluation of Anionic Phosphinoferrrocene Amidosulfonate Ligands. *Catalysts* **2017**, *7*, 167. [[CrossRef](#)]
42. Waldo, J.P.; Larock, R.C. The Synthesis of Highly Substituted Isoxazoles by Electrophilic Cyclization: An Efficient Synthesis of Valdecocixib. *J. Org. Chem.* **2007**, *72*, 9643–9647. [[CrossRef](#)]
43. Karadeniz, E.; Zora, M.; Kılıçaslan, N.Z. Facile synthesis of aryl-substituted pyridines via Suzuki–Miyaura approach. *Tetrahedron* **2015**, *71*, 8943–8952. [[CrossRef](#)]
44. O’Brien, C.J.; Kantchev, E.A.B.; Valente, C.; Hadei, N.; Chass, G.A.; Lough, A.; Hopkinson, A.C.; Organ, M.G. Easily Prepared Air- and Moisture-Stable Pd–NHC (NHC=N-Heterocyclic Carbene) Complexes: A Reliable, User-Friendly, Highly Active Palladium Precatalyst for the Suzuki–Miyaura Reaction. *Chem.–Eur. J.* **2006**, *12*, 4743–4748. [[CrossRef](#)]
45. Perdew, J.P.; Wang, Y. Accurate and simple analytic representation of the electron-gas correlation energy. *Phys. Rev. B* **1992**, *45*, 13244–13249. [[CrossRef](#)]
46. Godbout, N.; Salahub, D.R.; Andzelm, J.; Wimmer, E. Optimization of Gaussian-type basis sets for local spin density functional calculations. Part I. Boron through neon, optimization technique and validation. *Can. J. Chem.* **1992**, *70*, 560–571. [[CrossRef](#)]
47. Paier, J.; Marsman, M.; Kresse, G. Why does the B3LYP hybrid functional fail for metals? *J. Chem. Phys.* **2007**, *127*, 024103. [[CrossRef](#)]
48. Ongagna, J.M.; Fouegue, A.D.T.; Amana, B.A.; D’Ambassa, G.M.; Mfomo, J.Z.; Meva’A, L.M.; Mama, D.B. B3LYP, M06 and B3PW91 DFT assignment of nd8 metal-bis-(N-heterocyclic carbene) complexes. *J. Mol. Model.* **2020**, *26*, 246. [[CrossRef](#)]
49. Peng, C.; Schlegel, H.B. Combining Synchronous Transit and Quasi-Newton Methods to Find Transition States. *Isr. J. Chem.* **1993**, *33*, 449–454. [[CrossRef](#)]
50. Tomasi, J.; Mennucci, B.; Cancès, E. The IEF version of the PCM solvation method: An overview of a new method addressed to study molecular solutes at the QM ab initio level. *J. Mol. Struct. THEOCHEM* **1999**, *464*, 211–226. [[CrossRef](#)]
51. Chung, H.-A.; Kang, Y.-J.; Chung, J.-W.; Cho, S.-D.; Yoon, Y.-J. Retro-ene reaction. V. Functionalization of 4,5-dihalopyridazin-6-ones using 1-hydroxymethyl-4,5-dihalopyridazin-6-ones as 1-0, 3-n, 5-0 ene-adducts. *J. Heterocycl. Chem.* **1999**, *36*, 277–281. [[CrossRef](#)]
52. Krajsovsky, G.; Károlyhazy, L.; Dunkel, P.; Boros, S.; Grillo, A.; Mátyus, P. Suzuki-aza-Wittig, Suzuki-condensation and aza-Wittig-electrocyclic ring-closure tandem reactions for synthesis of fused nitrogen-containing ring systems. *Arkivoc* **2011**, *2011*, 229. [[CrossRef](#)]
53. Ganley, J.M.; Waller, D.L. Synthesis of Furo[2,3-c]pyridazines via Tandem Transition-Metal Catalysis. *J. Org. Chem.* **2017**, *82*, 12740–12745. [[CrossRef](#)]
54. Yu, M.; Ledebor, M.W.; Daniels, M.; Malojcic, G.; Tibbitts, T.T.; Gal, M.C.-L.; Pan-Zhou, X.-R.; Westerling-Bui, A.; Beconi, M.; Reilly, J.F.; et al. Discovery of a Potent and Selective TRPC5 Inhibitor, Efficacious in a Focal Segmental Glomerulosclerosis Model. *ACS Med. Chem. Lett.* **2019**, *10*, 1579–1585. [[CrossRef](#)]
55. Miyaura, N.; Suzuki, A. Palladium-Catalyzed Cross-Coupling Reactions of Organoboron Compounds. *Chem. Rev.* **1995**, *95*, 2457–2483. [[CrossRef](#)]
56. Amatore, C.; Jutand, A.; Le Duc, G. Kinetic Data for the Transmetalation/Reductive Elimination in Palladium-Catalyzed Suzuki–Miyaura Reactions: Unexpected Triple Role of Hydroxide Ions Used as Base. *Chem.–Eur. J.* **2011**, *17*, 2492–2503. [[CrossRef](#)]
57. Molloy, J.J.; Seath, C.P.; West, M.J.; McLaughlin, C.; Fazakerley, N.J.; Kennedy, A.R.; Nelson, D.J.; Watson, A.J.B. Interrogating Pd(II) Anion Metathesis Using a Bifunctional Chemical Probe: A Transmetalation Switch. *J. Am. Chem. Soc.* **2017**, *140*, 126–130. [[CrossRef](#)]
58. Miyaura, N.; Yamada, K.; Suginome, H.; Suzuki, A. Novel and convenient method for the stereo- and regioselective synthesis of conjugated alkadienes and alkenynes via the palladium-catalyzed cross-coupling reaction of 1-alkenylboranes with bromoalkenes and bromoalkynes. *J. Am. Chem. Soc.* **1985**, *107*, 972–980. [[CrossRef](#)]
59. Matos, K.; Soderquist, J.A. Alkylboranes in the Suzuki–Miyaura Coupling: Stereochemical and Mechanistic Studies. *J. Org. Chem.* **1998**, *63*, 461–470. [[CrossRef](#)]
60. Carrow, B.P.; Hartwig, J.F. Distinguishing Between Pathways for Transmetalation in Suzuki–Miyaura Reactions. *J. Am. Chem. Soc.* **2011**, *133*, 2116–2119. [[CrossRef](#)]

61. Jover, J.; Fey, N.; Purdie, M.; Lloyd-Jones, G.; Harvey, J.N. A computational study of phosphine ligand effects in Suzuki–Miyaura coupling. *J. Mol. Catal. A Chem.* **2010**, *324*, 39–47. [[CrossRef](#)]
62. Braga, A.; Morgon, N.H.; Ujaque, G.; Lledos, A.; Maseras, F. Computational study of the transmetalation process in the Suzuki–Miyaura cross-coupling of aryls. *J. Organomet. Chem.* **2006**, *691*, 4459–4466. [[CrossRef](#)]
63. Thomas, A.A.; Wang, H.; Zahrt, A.F.; Denmark, S.E. Structural, Kinetic, and Computational Characterization of the Elusive Arylpalladium(II)boronate Complexes in the Suzuki–Miyaura Reaction. *J. Am. Chem. Soc.* **2017**, *139*, 3805–3821. [[CrossRef](#)] [[PubMed](#)]
64. Cornelio, B.; Saunders, A.R.; Solomonsz, W.A.; Laronze-Cochard, M.; Fontana, A.; Sapi, J.; Khlobystov, A.N.; Rance, G.A. Palladium nanoparticles in catalytic carbon nanoreactors: The effect of confinement on Suzuki–Miyaura reactions. *J. Mater. Chem. A* **2015**, *3*, 3918–3927. [[CrossRef](#)]
65. Navarro, O.; Kaur, H.; Mahjoor, P.; Nolan, S.P. Cross-coupling and dehalogenation reactions catalyzed by (N-heterocyclic carbene)Pd(allyl)Cl complexes. *J. Org. Chem.* **2004**, *69*, 3173–3180. [[CrossRef](#)] [[PubMed](#)]
66. Viciu, M.S.; Grasa, G.A.; Nolan, S.P. Catalytic Dehalogenation of Aryl Halides Mediated by a Palladium/Imidazolium Salt System. *Organometallics* **2001**, *20*, 3607–3612. [[CrossRef](#)]
67. Ahmadi, Z.; McIndoe, J.S. A mechanistic investigation of hydrodehalogenation using ESI-MS. *Chem. Commun.* **2013**, *49*, 11488–11490. [[CrossRef](#)]
68. Moon, J.; Lee, S. Palladium catalyzed-dehalogenation of aryl chlorides and bromides using phosphite ligands. *J. Organomet. Chem.* **2009**, *694*, 473–477. [[CrossRef](#)]
69. Zeng, M.; Du, Y.; Shao, L.; Qi, C.; Zhang, X.-M. Palladium-Catalyzed Reductive Homocoupling of Aromatic Halides and Oxidation of Alcohols. *J. Org. Chem.* **2010**, *75*, 2556–2563. [[CrossRef](#)]
70. Vikse, K.L.; Ahmadi, Z.; Manning, C.C.; Harrington, D.A.; McIndoe, J.S. Powerful Insight into Catalytic Mechanisms through Simultaneous Monitoring of Reactants, Products, and Intermediates. *Angew. Chem. Int. Ed.* **2011**, *50*, 8304–8306. [[CrossRef](#)]
71. Sato, M.; Shigeta, H.; Sekino, M.; Akabori, S. Synthesis, some reactions, and molecular structure of the Pd(BF₄)₂ complex of 1,1'-bis(diphenylphosphino)ferrocene. *J. Organomet. Chem.* **1993**, *458*, 199–204. [[CrossRef](#)]
72. Klapp, L.R.R.; Bruhn, C.; Leibold, M.; Siemeling, U. Ferrocene-Based Bis(guanidines): Superbases for Tridentate N,Fe,N-Coordination. *Organometallics* **2013**, *32*, 5862–5872. [[CrossRef](#)]
73. Bárta, O.; Gyepes, R.; Císařová, I.; Alemayehu, A.; Štěpnička, P. Synthesis and study of Fe → Pd interactions in unsymmetric Pd(ii) complexes with phosphiniferrocene guanidine ligands. *Dalton Trans.* **2020**, *49*, 4225–4229. [[CrossRef](#)]
74. Metallinos, C.; Tremblay, D.; Barrett, F.B.; Taylor, N.J. 1,1'-Bis(phosphoranylideneamino)ferrocene palladium(II) complexes: An unusual case of dative Fe → Pd bonding. *J. Organomet. Chem.* **2006**, *691*, 2044–2047. [[CrossRef](#)]
75. Abubekero, M.; Khan, S.I.; Diaconescu, P.L. Ferrocene-bis(phosphinimine) Nickel(II) and Palladium(II) Alkyl Complexes: Influence of the Fe–M (M = Ni and Pd) Interaction on Redox Activity and Olefin Coordination. *Organometallics* **2017**, *36*, 4394–4402. [[CrossRef](#)]
76. Jess, K.; Baabe, D.; Bannenberg, T.; Brandhorst, K.; Freytag, M.; Jones, P.G.; Tamm, M. Ni–Fe and Pd–Fe Interactions in Nickel(II) and Palladium(II) Complexes of a Ferrocene-Bridged Bis(imidazolin-2-imine) Ligand. *Inorg. Chem.* **2015**, *54*, 12032–12045. [[CrossRef](#)]
77. Fabricant, R.N.; De Larco, J.E.; Todaro, G.J. Nerve growth factor receptors on human melanoma cells in culture. *Proc. Natl. Acad. Sci. USA* **1977**, *74*, 565–569. [[CrossRef](#)]
78. Giard, D.J.; Aaronson, S.A.; Todaro, G.J.; Arnstein, P.; Kersey, J.H.; Dosik, H.; Parks, W.P. In Vitro Cultivation of Human Tumors: Establishment of Cell Lines Derived From a Series of Solid Tumors. *JNCI J. Natl. Cancer Inst.* **1973**, *51*, 1417–1423. [[CrossRef](#)]
79. Pontén, J.; Macintyre, E.H. LONG TERM CULTURE OF NORMAL AND NEOPLASTIC HUMAN GLIA. *Acta Pathol. Microbiol. Scand.* **1968**, *74*, 465–486. [[CrossRef](#)]
80. Knowles, B.B.; Aden, D.P. Human Hepatoma Derived Cell Line, Process for Preparation Thereof, and Uses Therefor. U.S. Patent 4393133A, 12 July 1983.
81. Frisch, G.W.; Trucks, H.B.; Schlegel, G.E.; Scuseria, M.A.; Robb, J.R.; Cheeseman, G.; Scalmani, V.; Barone, G.A.; Petersson, H.; Nakatsuji, X. *Gaussian*; Revision C.01; Gaussian Inc.: Wallingford, CT, USA, 2016.
82. Slater, T.F.; Sawyer, B.; Sträuli, U. Studies on succinate-tetrazolium reductase systems: III. Points of coupling of four different tetrazolium salts III. Points of coupling of four different tetrazolium salts. *Biochim. Biophys. Acta (BBA)-Bioenerg.* **1963**, *77*, 383–393. [[CrossRef](#)]
83. Liu, Y.; Peterson, D.A.; Kimura, H.; Schubert, D. Mechanism of Cellular 3-(4,5-Dimethylthiazol-2-yl)-2,5-Diphenyltetrazolium Bromide (MTT) Reduction. *J. Neurochem.* **2002**, *69*, 581–593. [[CrossRef](#)]
84. Altman, F.P. Tetrazolium salts and formazans. *Prog. Histochem. Cytochem.* **1976**, *9*, 1–56. [[CrossRef](#)]
85. Denizot, F.; Lang, R. Rapid colorimetric assay for cell growth and survival. Modifications to the tetrazolium dye procedure giving improved sensitivity and reliability. *J. Immunol. Methods* **1986**, *89*, 271–277. [[CrossRef](#)]